AD/A-005 324

WING PRESSURE DISTRIBUTION AND BOUNDARY LAYER DATA OBTAINED FROM C-5A FLIGHT TESTING

Jones F. Cahill, et al

Lockheed-Georgia Company

Prepared for:

Aerospace Research Laboratories

October 1974

DISTRIBUTED BY:

NTIS

National Technical Information Service
U. S. DEPARTMENT OF COMMERCE
5285 Port Royal Road, Springfield Va. 22151

UNCLASSIFIED

SECURITY CLASSIFICATION OF THIS PAGE (When Data Entered)

REPORT DOCUMENTATION PAGE		READ INSTRUCTIONS BEFORE COMPLETING FORM
1. REPORT NUMBER ARL 74-0117	2. GOVT ACCESSION NO.	3. RECIPIENT'S CATALOG NUMBER AD/A-005 447
4. TITLE (and Subtitle) WING PRESSURE DISTRIBUTION AND BOUNDARY LAYER DATA OBTAINED FROM C-5A FLIGHT TESTING		5. TYPE OF REPORT & PERIOD COVERED Technical - Final JULY 73 - FEBRUARY 74
		6. PERFORMING ORG. REPORT NUMBER Lockheed Ga. Rept LG74ER0071
7. AUTHOR(s) JONES F. CAHILL WILLIAM A. STEVENS		8. CONTRACT OR GRANT NUMBER(s) CONTRACT NUMBER F33615-73-C-4168
9. PERFORMING ORGANIZATION NAME AND ADDRESS LOCKHEED-GEORGIA COMPANY A DIVISION OF THE LOCKHEED AIRCRAFT CORP. MARIETTA, GEORGIA 30063		10. PROGRAM ELEMENT, PROJECT, TASK AREA & WORK UNIT NUMBERS 61102F; 7064-02-06
11. CONTROLLING OFFICE NAME AND ADDRESS Aerospace Research Laboratories (LH) Air Force Systems Command Wright-Patterson AF Base, Ohio 45433		12. REPORT DATE October 1974
		13. NUMBER OF PAGES 90
14. MONITORING AGENCY NAME & ADDRESS(if different from Controlling Office)		15. SECURITY CLASS (of this report) UNCLASSIFIED
		15a. DECLASSIFICATION/DOWNGRADING SCHEDULE

16. DISTRIBUTION STATEMENT (of this Report)

Approved for public release; distribution unlimited.

17. DISTRIBUTION STATEMENT (of the abstract entered in Block 20, if different from Report)

DDC

18. SUPPLEMENTARY NOTES

19. KEY WORDS (Continue on reverse side if necessary and identify by block number)

transonic flow
shock - boundary layer interaction
turbulent boundary layer
turbulent skin friction

20. ABSTRACT (Continue on reverse side if necessary and identify by block number)

Analyses have been conducted of wing pressure distribution and boundary layer data obtained from flight tests of a C-5 airplane at Reynolds numbers from 35 to 90 million. Results showed that shock locations at high subsonic Mach numbers are as much as 10 to 12 percent chord aft of those measured in previous wind tunnel tests at 7.4 million Reynolds number. No consistent variation in shock location with Reynolds number within the range covered by the flight data can be detected, however. Consideration of the boundary

DD FORM 1 JAN 73 1473 EDITION OF 1 NOV 65 IS OBSOLETE

SECURITY CLASSIFICATION OF THIS PAGE (When Data Entered)

20. continued

layer data in conjunction with the pressure measurements would indicate that this absence of scale effects at high Reynolds number results from the fact that trailing-edge separation is suppressed to the extent that separation at the shock is the dominant factor leading to flow breakdown.

Comparisons of the measured boundary layer data with several theoretical predictions disclosed no unusual characteristics attributable to the high Reynolds number of the tests.

PREFACE

This report was prepared in the Aerodynamics Department of the Lockheed-Georgia Company for the Aerospace Research Laboratories, Air Force Systems Command, United States Air Force Project 7064 entitled "High Velocity Fluid Mechanics," Project Monitor - Dr. R. H. Korkegi, under Contract F33615-73-C-4168. Lieutenant Michael Freeman served as Air Force program monitor. Appreciation is due to the Engineering Test Division of the Lockheed-Georgia Company for their special efforts in conducting the flight testing which provided the data used in this study. That testing was funded by the C-5A System Project Office, Aeronautical Systems Division, under Contract F33615-71-A-0083-0008, with Mr. John R. Hagerman acting as program monitor.

Boundary layer rakes used in the flight test program were provided by the NASA Flight Research Center. Their cooperation in this regard is sincerely appreciated.

This report is also identified as Lockheed-Georgia Company Report LG74ER0071.

TABLE OF CONTENTS

LIST OF TABLES

LIST OF ILLUSTRATIONS

LIST OF ILLUSTRATIONS (Continued)

LIST OF ILLUSTRATIONS (Continued)

LIST OF SYMBOLS

a	Local speed of sound
b	Wing span
c	Local chord
$\bar{c}$	Mean aerodynamic chord
C_p	Pressure coefficient, $\Delta P/q$
C_f	Skin friction coefficient, τ_w/q_e
H	Total pressure
M	Mach number
M_{un}	Mach number normal to the wing element lines
P	Static pressure
P_r	Prandtl number
q	Dynamic pressure, $\frac{\gamma}{2} PM^2$
r	Recovery factor
R_N	Reynolds number, $\frac{\rho_\infty U_\infty \bar{c}}{\mu_\infty}$
T	Static temperature, ^oR
u	Local velocity
u^*	Shear velocity, $\sqrt{\tau_w/\rho e}$
x/c	Nondimensional chordwise location
y	Distance normal to the wing surface
α	Correlation angle of attack (see Figure 7)
α_{FRL}	Aircraft angle of attack
γ	Ratio of specific heats, 1.4
Γ	Flow direction angle, degrees measured laterally from aircraft centerline

δ	Boundary layer thickness
δ^*	Displacement thickness, $\int_0^\delta \left(1 - \frac{\rho u}{\rho_e u_e} \, dy\right)$
η	Nondimensional semispan station
θ	Momentum thickness, $\int_0^\delta \frac{\rho u}{\rho_e u_e} \left(1 - \frac{u}{u_e} \, dy\right)$
μ	Absolute viscosity
ν	Kinematic viscosity, μ/ρ
ρ	Density
τ_w	Wall shear

Subscripts

e	Edge of the boundary layer
ℓ	Local
s	Freestream static
T	Indicates total temperature
y	Local boundary-layer condition at height y above the surface
EXP	Experimental
2-D	Two-dimensional theory

SECTION I

INTRODUCTION

The questions associated with scale effects in transonic aerodynamics have assumed increasing importance in recent years. Those aspects of transonic scaling involving shock-induced separations have been widely discussed and are illustrated by data measured in 1968 on the Lockheed C-141 airplane. In contrast with prior experience, these data showed that large differences in chordwise load distribution were caused by differences between wind tunnel and flight Reynolds numbers. Figure 1 shows the variation of shock location with Reynolds number for the C-141 and the correlation between shock location change and rear separation as indicated by trailing-edge pressure recovery. The change in shock location shown in Figure 1 approximately doubled the section pitching moment coefficient, and is, therefore, very significant in defining structural loads. Pearcey (in Reference 1) discusses the basic phenomena involved in this kind of transonic scaling effects.

Figure 2 illustrates the various component phenomena which combine to produce the net scale effects which have been observed.

- At the shock, a separation will occur if the local Mach number forward of the shock is sufficiently great.

- Because of curvatures introduced into the flow field by flow approaching the separation region, the lower portion of the shock is probably composed of a series of relatively weak oblique compression waves, rather than a strong normal shock. The sonic line may, therefore, extend well downstream of the shock near the surface.

- The flow generally reattaches downstream of the shock, enclosing a bubble of separated flow.

- The reattached boundary layer relaxes into conventional velocity distributions and may separate again in the adverse pressure gradient approaching the trailing edge.

Pearcey presented in Reference 1 a classification of types of flow, divided primarily between Model A, those for which the trailing-edge separation resulted from an aft growth of the shock-induced separation bubble, and Model B, those for which the trailing-edge separation spread forward because of aft pressure gradient effects. As confirmed by Reference 1 and a number of other studies, the local separation at the shock shows only a minimal response to changes in Reynolds number, while the rear separation is likely to show strong responses.

The manner in which trailing-edge separation causes a change in shock location is shown in Figure 3. In this figure (taken from Reference 2), wind-tunnel data are shown for a fixed Reynolds number of approximately 3 million, based on wing mean aerodynamic chord. The data for the bare model show a trailing-edge separation which results in a

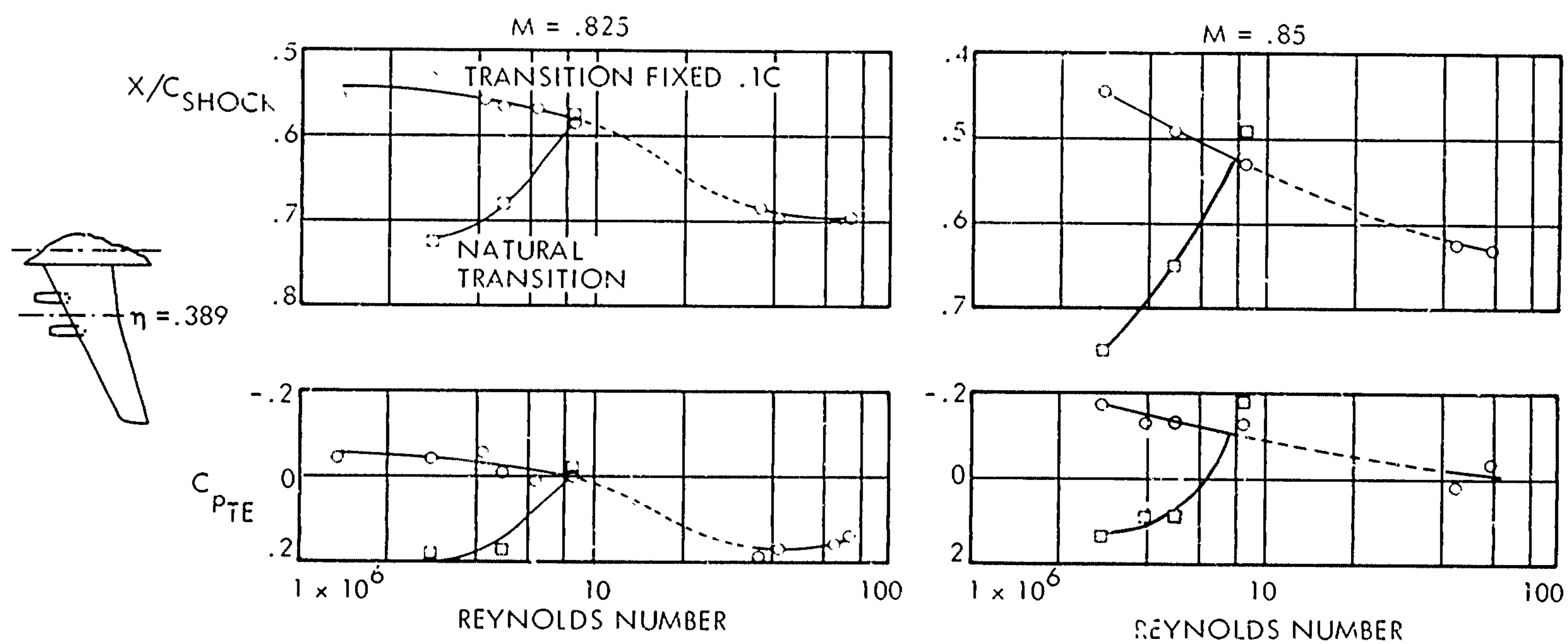

Figure 1. Scale Effects on Transonic Shock-Induced Separation

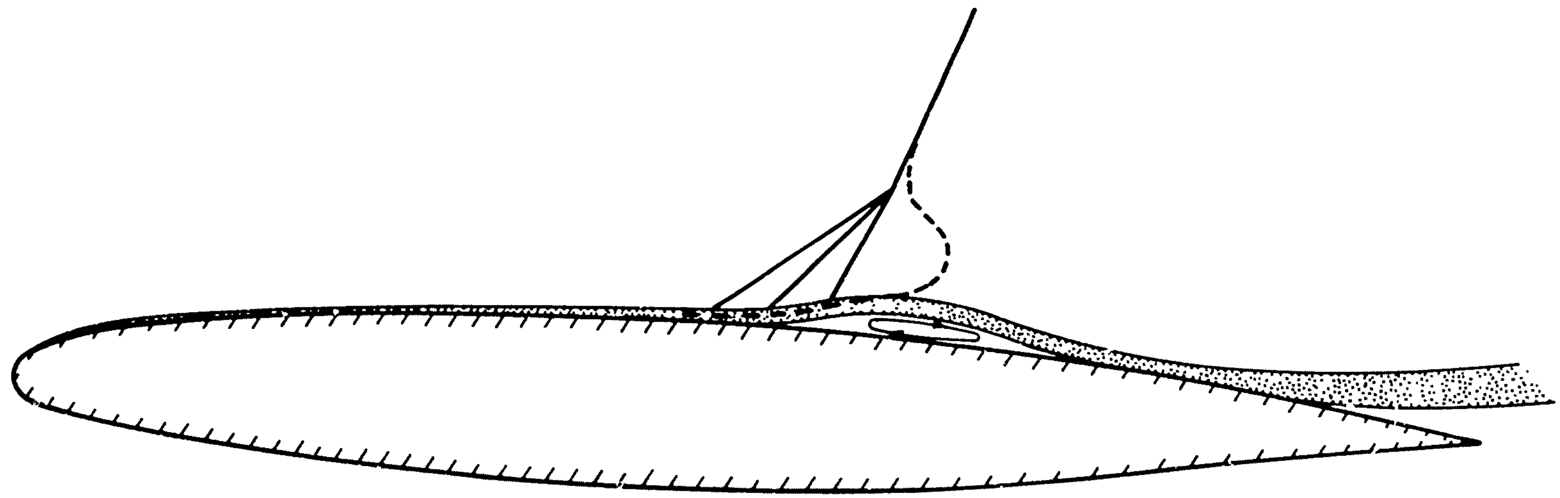

Figure 2. Shock-Induced Separation Phenomena

VORTEX GENERATORS
BEHIND SHOCK

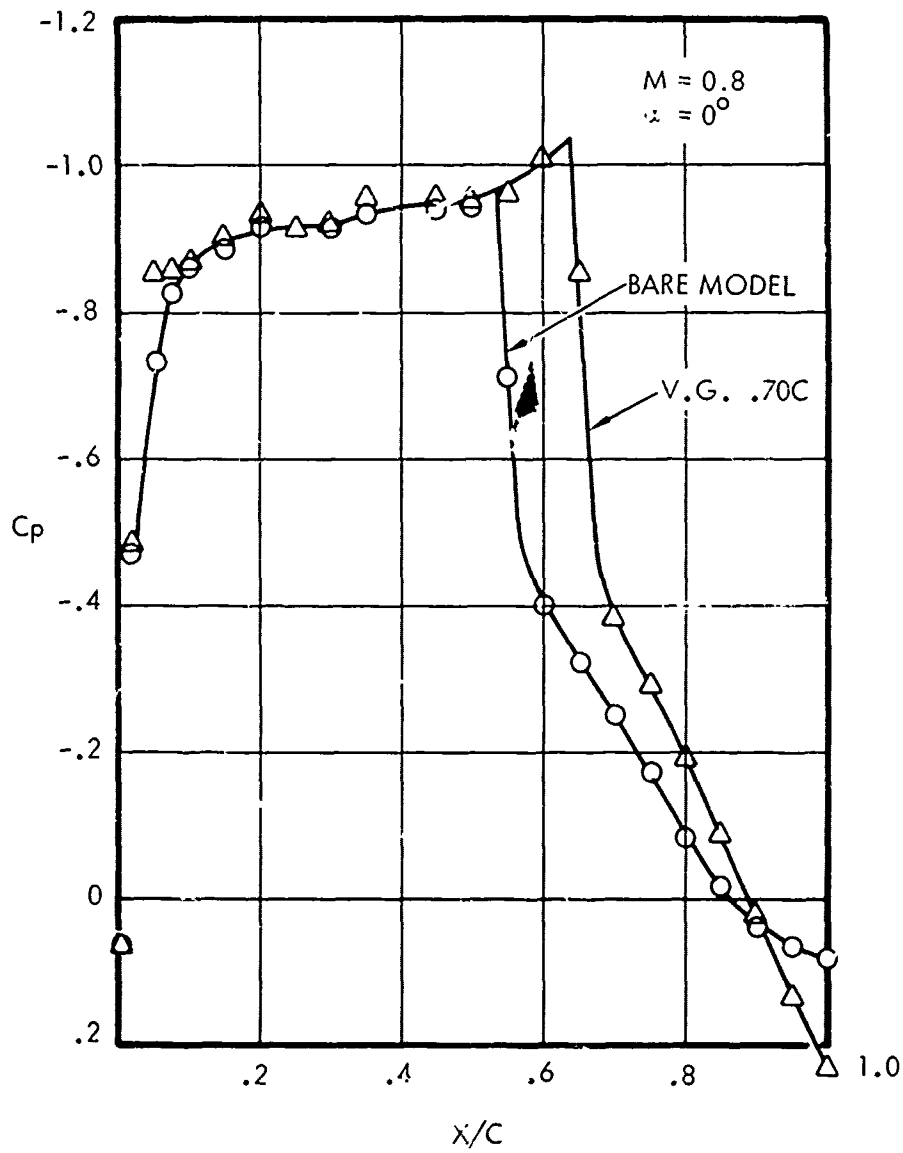

Figure 3. Trailing Edge Separation Effects

modification of the entire subsonic velocity distribution downstream of the shock. Addition of vortex generators behind the shock (at 70% chord) eliminates the trailing-edge separation and restores the downstream velocity distribution. Since the shock must establish a reconciliation between the upstream supersonic flow and the downstream subsonic flow, the downstream velocity distribution changes resulting from trailing-edge separation must cause shock location changes.

In recognition of the large differences in aerodynamic characteristics which can occur as a result of differences in Reynolds number, intensive current development efforts are aimed at the eventual construction of high Reynolds number wind tunnels. Future evaluation of data from those tunnels would be enhanced by the existence of very high Reynolds number data on a practical flight vehicle. Presence of the C-5A in an ongoing flight test program provided an opportunity to obtain some data on wing pressure distributions and boundary layer characteristics which might supply at least a portion of the data to be used for future high Reynolds number tunnel evaluation.

This report contains an analysis of those data with the objectives of, first, showing whatever scale effects might exist and, second, correlating the measured boundary layer data against existing theories, to show the validity of this approach as a tunnel data evaluation basis.

SECTION II

EXPERIMENTAL DATA

Data for this analysis were obtained concurrently with other planned flight test work on a C-5A airplane during 1973. The basic objective was to obtain a limited amount of wing pressure distribution and boundary layer data over the widest possible range of Reynolds number for flight conditions in which scale effect differences might occur. This section reviews briefly the instrumentation used for these measurements, data reduction procedures, and the scope of data obtained.

1. INSTRUMENTATION

Figure 4 shows the overall lay out of instrumentation used to measure the data for this study. Chordwise pressure distributions were measured at wing stations 592 and 921 on the right wing. Multiple-tube plastic strips (called "strip-a-tube") were bonded to the wing surface at those spanwise stations. Holes punched into the tubes formed static pressure orifices for measuring pressure distributions. The tubes were connected to scanivalves which were installed in the cavity under the wing spoilers. The scanivalves were timed to sense 48 individual pressures in a 2-1/2 second scan time. All pressures were referred to a reservoir also installed in the spoiler cavity. Wing stations 592 and 921 were selected for measurements in this program because they represent two potentially different flow situations. Station 592 is a spanwise position roughly midway between the inboard and outboard engines. Station 921 is sufficiently removed from fuselage and engine locations to approximate "infinite yawed wing" conditions. "Strip-a-tube" has been used in this way in previous studies and has indicated no distortion of measured data.

Boundary layer properties were measured at the same spanwise stations on the left wing, at 40% and at 75% of the local wing chord. At each of those four locations, a total pressure rake, a thermocouple rake, a Preston tube, and a local static pressure orifice were installed.

The upper photograph in Figure 5 shows a typical installation at the forward locations (40% chord). The Preston tube appears in the lower right-hand corner and contains the local static pressure orifice also. The lower photograph in Figure 5 shows the rakes installed at 75% chord at wing station 921. The total pressure rake at this location consisted of two probes attached to a mast which was traversed through the boundary layer by a motor-driven screw. The traverse time for this rake was 11 seconds. Each of the probes on this rake, both of the aft Preston tubes, and approximately half the probes on the inboard aft total pressure rake, were directionally sensitive probes similar to that described in Reference 3. These probes consist of a central total pressure tube cut off square, with an additional tube on either side cut off at a 45-degree angle. Flow-direction angles are determined as a function of the difference in pressure indicated by the two diagonal tubes. The flow angles are then utilized with appropriate calibration curves to determine total

pressures in the direction parallel to the local flow direction. This procedure and the calibration curves are presented in detail in Reference 3. Boundary layer pressure data were sensed by scanivalves, except for the traversing probe data, which were sensed by differential pressure transducers and recorded continuously as the probe traversed the boundary layer.

The instrumentation system was calibrated for conventional lag effects which can occur when static pressures are changing rapidly. All data presented were corrected to account for these effects.

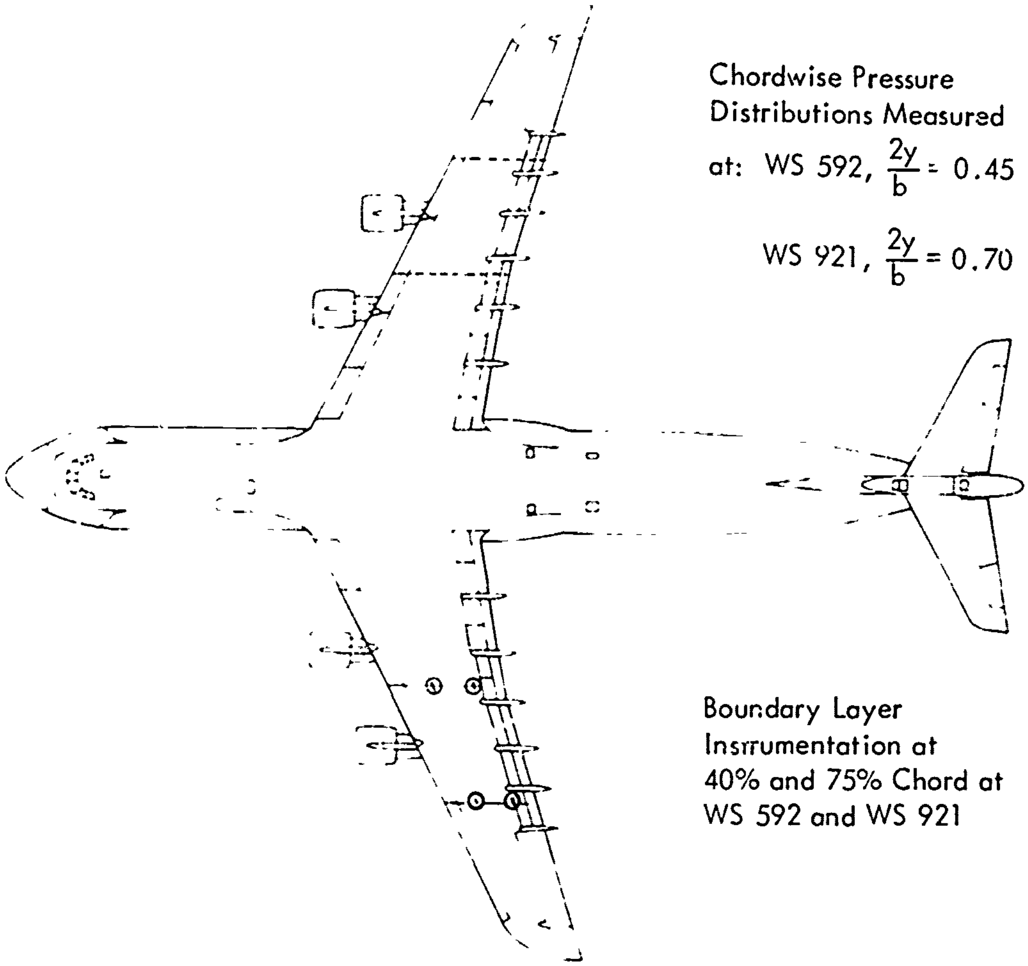

Figure 4. Planview of the C-5 Showing the Locations of the Strip-A-Tubing and Boundary Layer Instrumentation

W.S. 921 40% CHORD

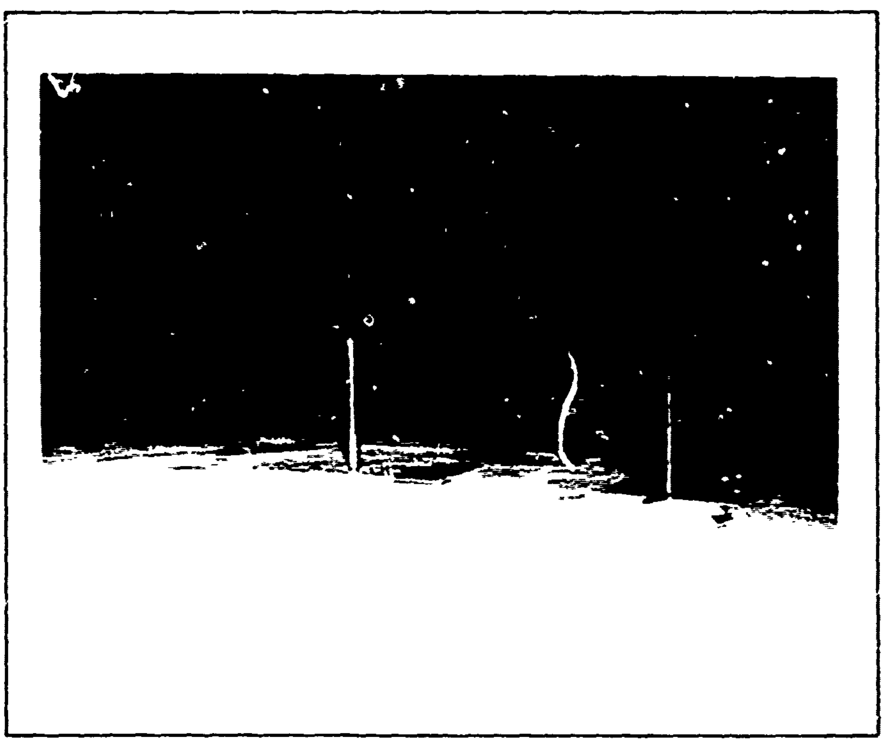

W.S. 921 75% CHORD

Figure 5. Photographs of Instrument Installations

Flight condition data were obtained from total and static pressure tubes mounted on a nose boom, and from an accelerometer mounted at the airplane center of gravity. All data were recorded on magnetic tape for a substantial time interval at each test condition. Using an interpolation routine, we read the data out of the tape at a single instant for each test condition. The measured data were reduced to aerodynamic coefficient form from conventional equations which are summarized below.

Pressure coefficient,

$$C_p = \frac{p_e - p_s}{q}$$

Boundary layer velocity,

$$U_y = M_y a_y = M_y 49\sqrt{T_e}$$

M_y is obtained from the local value of P/H_y, where p is the local surface static pressure, and H_y is local total pressure in the boundary layer.

$$p/H_y = \left(1 + \frac{M_y^2}{5}\right)^{-7/2} \qquad \text{(Subsonic)}$$

$$p/H_y = \left(\frac{6M_y^2}{5}\right)^{7/2} \left(\frac{6}{7M_y^2 - 1}\right)^{5/2} \qquad \text{(Supersonic)}$$

Boundary layer temperatures were sensed as total temperatures and converted to static temperatures by

$$T_y = \frac{T_T}{1 + .2M_y^2}$$

Wall temperature was calculated from the measured edge temperature with an assumed recovery factor of 0.88.

Preston tube pressure differences were converted to wall shear stress by using the calibration curve of Reference 4.

Values of the surface static pressure measured in the vicinity of the boundary layer probes showed rather large differences from those measured at the same location on the right wing, with the maximum discrepancy occurring adjacent to the probes. One attempt was made to eliminate this discrepancy by changing the relative location of the probes, but with no success. It is believed that the discrepancy is caused by disturbances due to the flow around the boundary layer pressure and temperature rakes. Therefore, the

boundary layer data were reduced by using the static pressure measured on the right wing. In all calculations it has been assumed that the static pressure is constant through the boundary layer.

2. ACCURACY

Overall accuracy of data presented in this report is affected by a large number of factors which are not well defined, and which vary from one test condition to another. Accuracy values shown are, therefore, qualitative estimates obtained from a cursory assessment of data scatter or repeatability.

Test Conditions:	M	± 0.003
	α	$\pm 0.1^{\circ}$
Measured Quantities:	C_p	± 0.02
	X/C_{SH}	± 0.01
	C_f	± 0.0001
	T	$\pm 1^{\circ}$
Derived Quantities:	δ^*, θ	± 0.003 Inches, Forward Rakes
		$\pm 4\%$ Aft Rakes

3 WING SURFACE CONDITION

One objective of the current study is to provide basic data for future correlation against high Reynolds number wind tunnel data. Therefore, surface condition of the airplane might well be a factor influencing such correlation. The basic surface of the wing of the test airplane is representative of normal aircraft manufacture. The surface of the wing between the forward and aft main spars (at 15% and 65% chord) is composed of a series of metal planks running approximately along the axis of the wing spars and having chord lengths of approximately 26 inches each. The joints between adjacent planks had small mismatches, resulting in steps which averaged ± 0.009 inch in height. The slat trailing edge forms an additional step at approximately 15% chord. This step-down varied considerably over the span of the wing, from a minimum of 0.050 to as much as 0.70 inch at some points. Of course, this discontinuity could be measured only on the ground, and the size of the step in flight is unknown. No leakage occurred through the gap at the slat trailing edge due to the presence of an internal seal.

4. DATA AVAILABLE

Many test points were available from the flight program. Test conditions had been planned to cover the widest possible range of Reynolds numbers for basic test conditions (Mach number and lift coefficient) for which Reynolds number effects might be anticipated.

Figure 6 shows Mach numbers, lift coefficients, and Reynolds numbers for which data were measured. Table I contains a listing of all of the test conditions and values of the correlation angle of attack, shock location, edge Mach number, skin friction coefficient, and the displacement and momentum thickness measured for those conditions.

All of the measured data were considered in some of the analyses contained in this report. In other cases, only a few points were selected to show the effects of the basic test-condition variables.

5. ANGLE OF ATTACK DEFINITION

Correlation of data of the type considered here, or isolation of individual influences within the data, is complicated by aeroelastic distortions of the wing. Local angle of attack (at any spanwise station) is influenced not only by gross weight, load factor, and dynamic pressure, but also by fuel loading, center of gravity, and any factor contributing to or modifying the structural deflection of the wing. Angles of attack used for correlation in this report are defined, therefore, in terms of the chordwise pressure distribution over the forward part of the airfoil section. To provide a practically useable method for defining angle of attack, the difference between upper and lower surface pressure coefficient at 30% chord was plotted against fuselage reference line angle of attack for one test series from previous wind tunnel testing (AEDC Test TF-179, Reference 5). These plots, shown in Figure 7 for the two wing stations for which flight data are available, then form the basis for definition of angle of attack at any given flight condition. Because of the aeroelastic twist, the effective angle of attack is generally different for the two spanwise stations. Figure 8 shows correlation of the complete pressure distribution for two cases for which the angles of attack are defined by using the plots of Figure 7. As shown by these comparisons, the entire forward part of the pressure distribution is matched very closely, even though shock locations and the extent of aft separation vary from case to case.

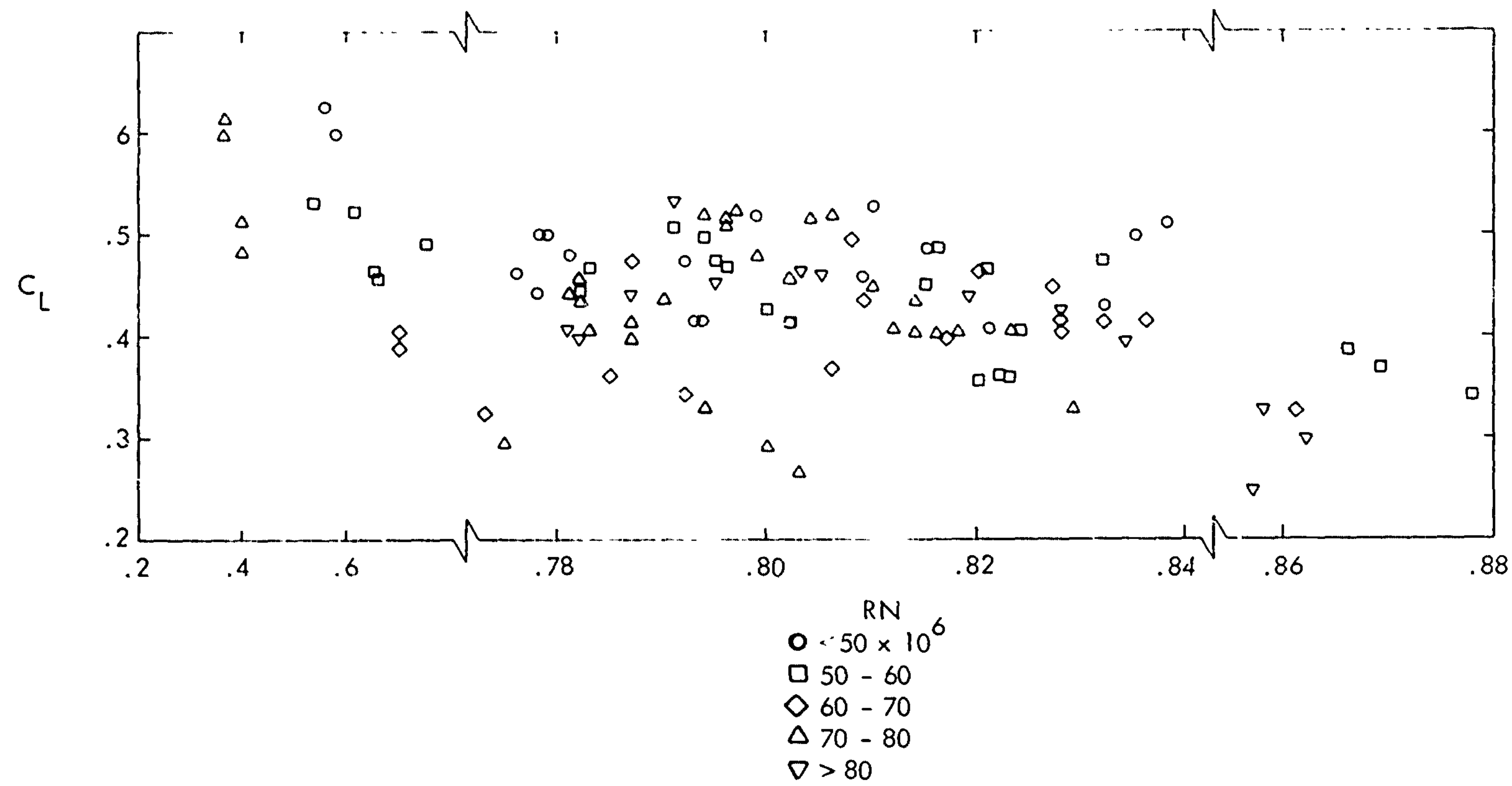

Figure 6. Summary of Flight Test Conditions

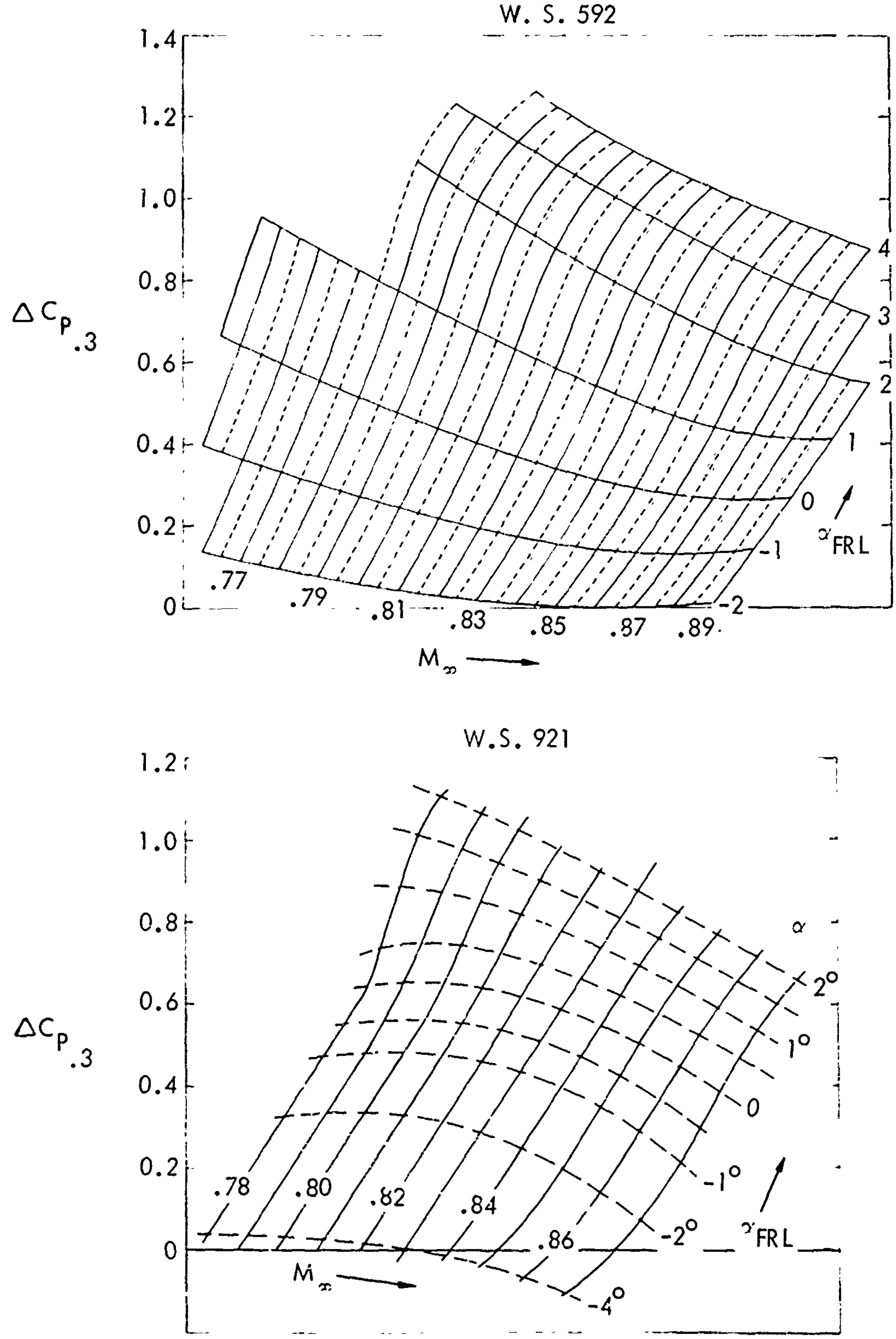

Figure 7. Angie of Attack Correlation

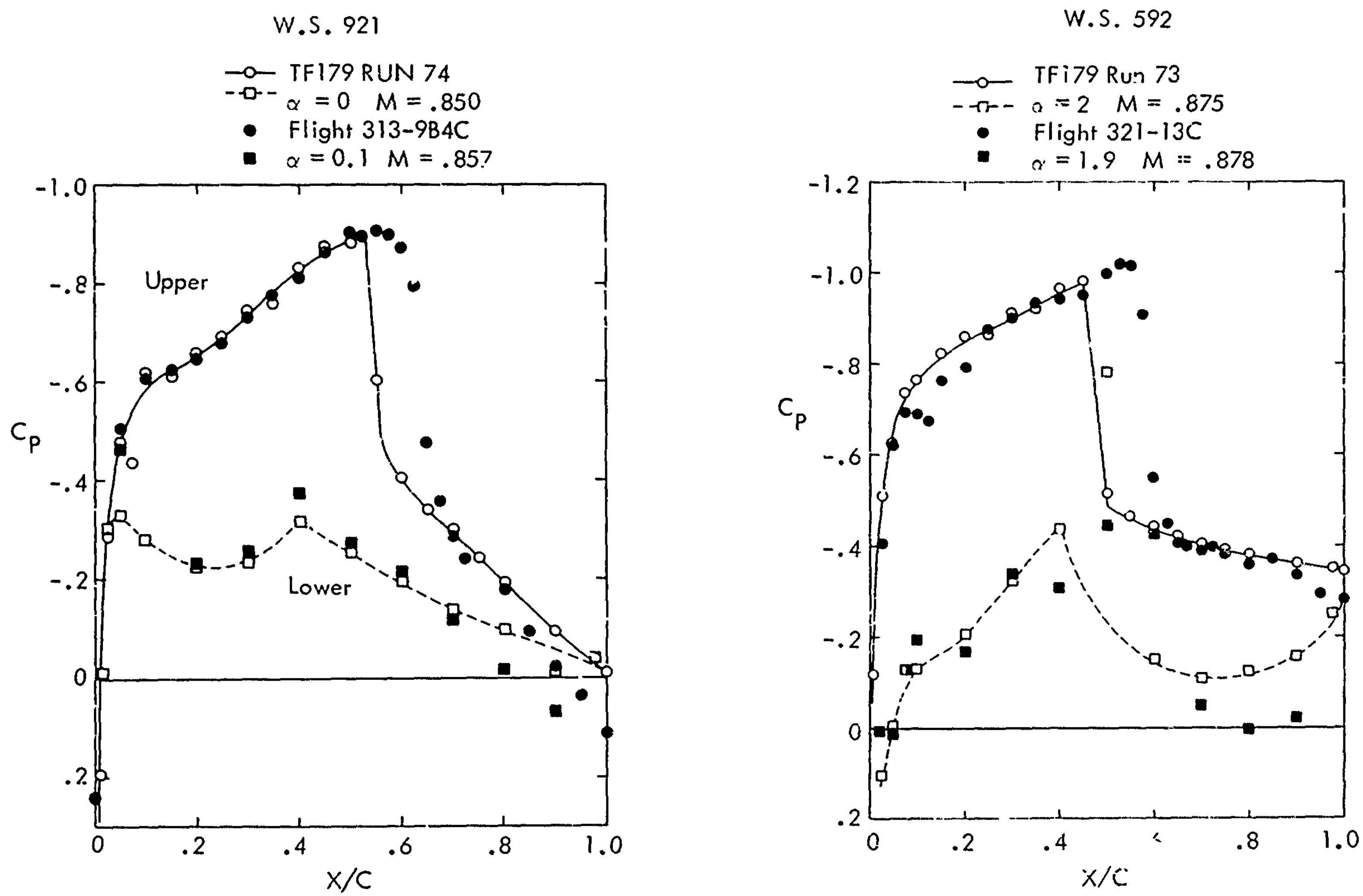

Figure 8. Comparison of Wind Tunnel and Flight Test Pressure Distributions Using the Angle of Attack Correlations

SECTION III

PRESSURE DISTRIBUTION DATA

Figures 9 and 10 show a sampling of pressure distributions measured at wing stations 592 and 921, respectively. These data are arranged to show the progressive changes in pressure distribution as angle of attack or Mach number is increased.

At the inboard station (wing station 592), the pressure distributions show evidence of a sharp but relatively weak compression in the flow forward of the strong shock which terminates the local supersonic flow field. These compressions are believed to result from flow disturbances originating at the leading-edge wing-fuselage juncture. Figure 12 (in the next section on boundary layer data) shows a sketch of this shock pattern on the planview of the wing for one test condition. The forward shock is more highly swept than the wing leading edge, and it merges with the terminal shock inboard of wing station 921. The forward shock also appears to move aft as either Mach number or angle of attack is increased, and it is not apparent in the data at high Mach number and α combinations.

Rather abrupt inflections appear in the pressure distributions near 10% chord on the upper and lower surfaces. These disturbances are probably caused by the slat misfit which produced the slat trailing-edge step discussed in Section II.

A progressive deterioration in trailing-edge pressure recovery is shown as the separation develops with increasing Mach number and angle of attack. Examination of the pressure distribution plots also shows the typical arresting of aft shock movement when the trailing-edge separation becomes apparent. These trends and the interaction of shock location change with rear separation will be examined in somewhat more detail in Section V.

Good correlation between pressure distribution measurements made in flight and wind tunnel testing has been demonstrated by the data shown in Figure 8. To verify data credibility, an analytical determination of the pressure distribution at wing station 592 was made for one test condition by using the viscous, infinite swept wing calculation method presented in Reference 6. Results of that computation are compared with wind tunnel data in Figure 11. The correlation shown is quite good, with minor distortions attributable to manufacturing tolerances, surface imperfections, or measuring accuracy.

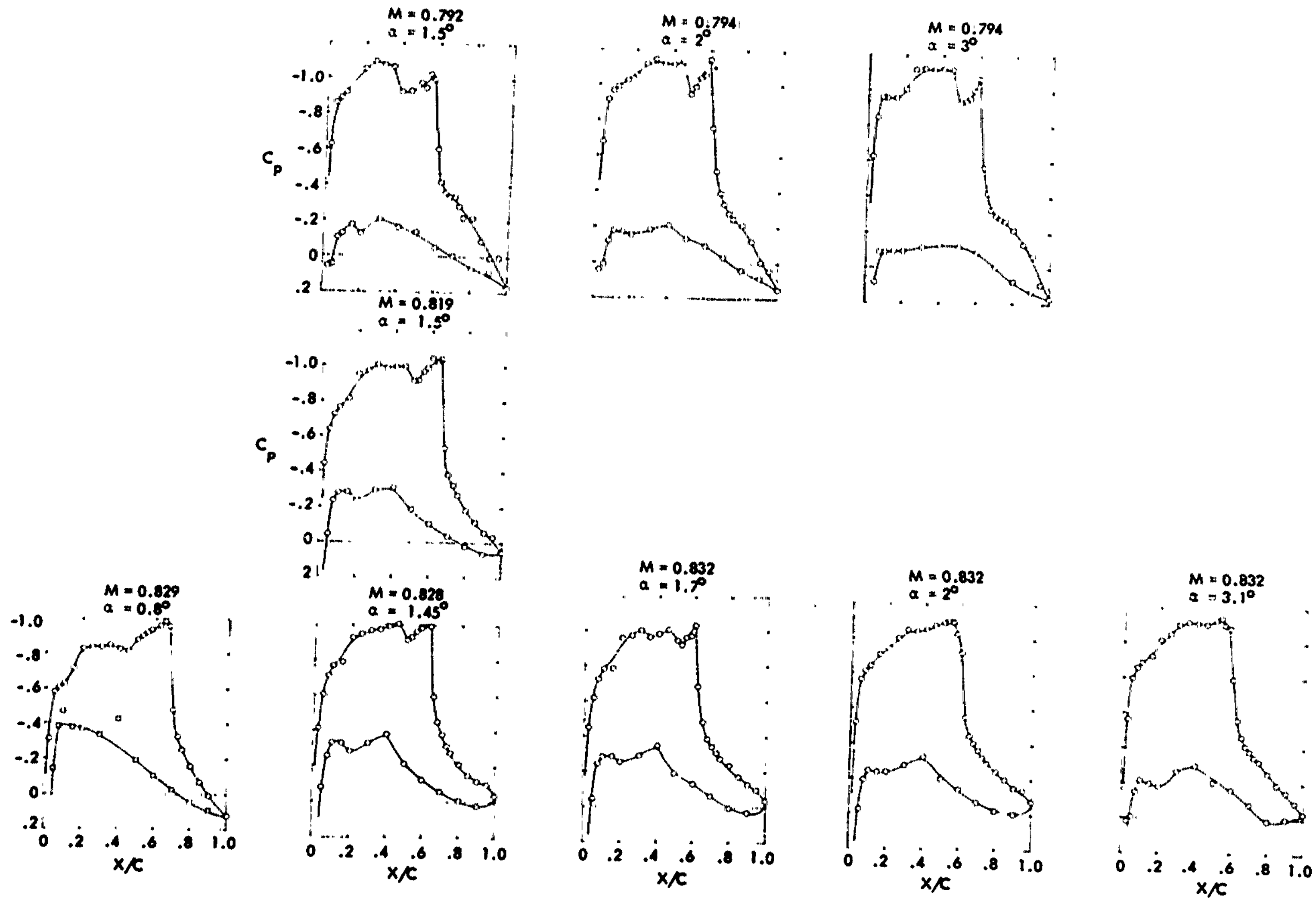

Figure 9. Typical Pressure Distributions as Affected by Changes in Mach Number and Angle of Attack. Wing Station 592

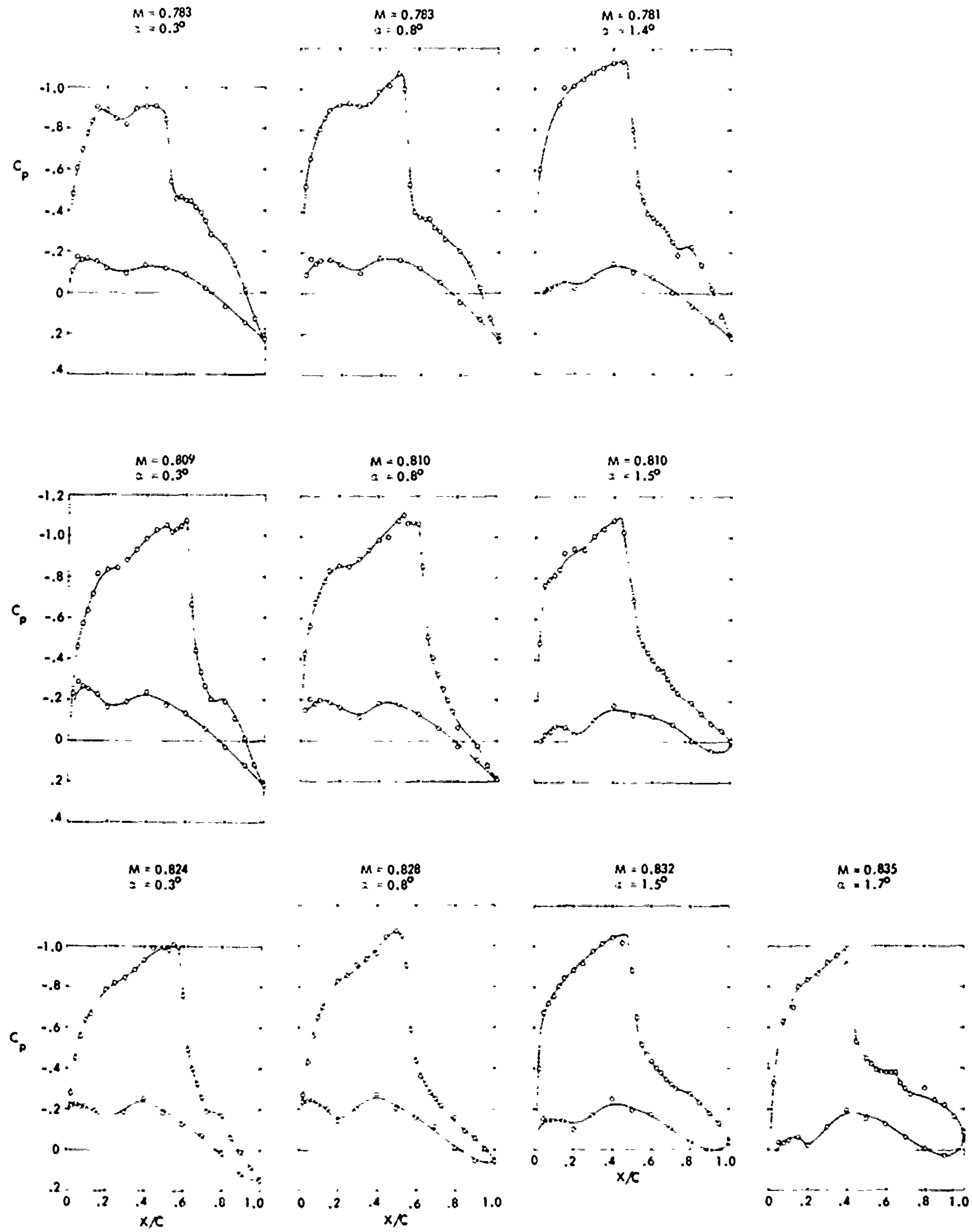

Figure 10. Typical Pressure Distributions as Affected by Changes in Mach Number and Angle of Attack. Wing Station 921

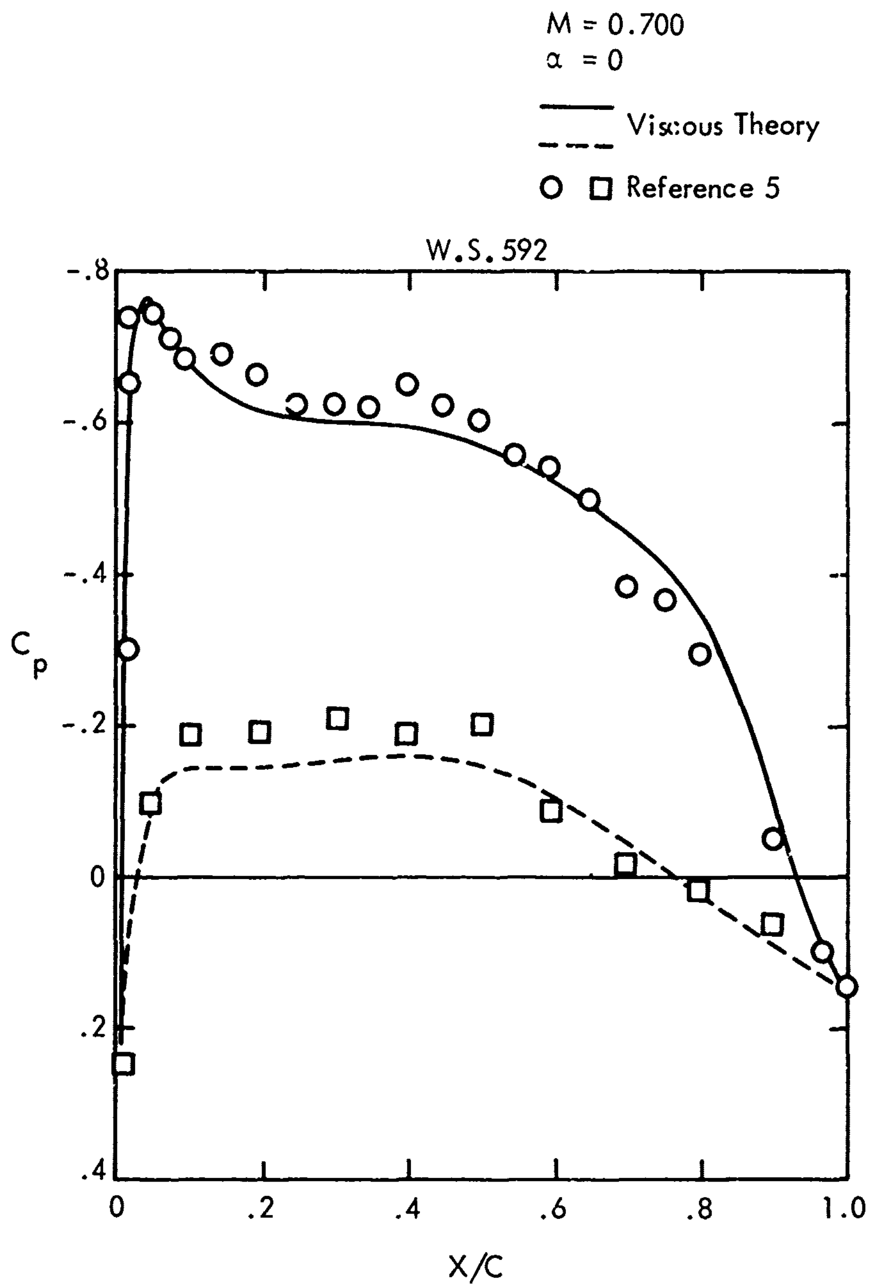

Figure 11. Comparison of Wind Tunnel Pressure Distribution with Viscous Theory Calculation

SECTION IV

BOUNDARY LAYER DATA

The boundary layer data considered here are subject to rather strong three-dimensional effects because of the airplane geometry, and because of significant spanwise variations in flow conditions at the transonic speeds which are of special interest in this study. It has not been possible to isolate the three-dimensional effects in any detail, but a brief review of the type of flow existing at these conditions may be useful in keeping the following results in their proper context.

Figure 12 shows a sketch of the shock pattern observed on the C-5A wing at one test condition in prior wind tunnel testing. Spanwise pressure gradients are introduced by the multiple shock system on the inboard wing, and further modified by disturbances at the wing leading edge-pylon intersections. Chordwise pressure distributions at a number of spanwise stations are shown in Figure 13. Plots of the pressure coefficients corresponding to local values of M_{un} equal to 1 are shown on each pressure distribution. The forward inboard shocks are shown to be relatively weak but sharp and distinct pressure rises. In most cases, the local velocities just aft of the terminal shock are quite close to sonic. For the two spanwise locations at which the flight data were measured ($\eta = 0.45$ and 0.7), both the flight and wind tunnel data are shown. Correlation between the flight and wind tunnel results is fairly good except for perturbations in the region of the leading-edge slat and a somewhat farther aft location of the forward shock at $\eta = 0.45$.

1. VELOCITY PROFILES

The pressure distribution data of Figure 13 were used as input to the three-dimensional turbulent boundary layer computing process developed by Nash and presented in Reference 7. Boundary layer profiles from that computation are compared with the experimental data for all four rakes in Figure 14. Comparison between theoretical and experimental results is quite good, although a rather significant distortion is apparent in the upper portion of the profile at wing station 592 aft. The source of that distortion cannot be identified from any measurements available for this study. However, similar velocity profiles are observed for other test points measured at similar Mach number and angle of attack conditions, and do not change with a change in Reynolds number. It is possible that this distorted profile results from a disturbance introduced at the wing-pylon juncture or by adjacent instrumentation.

Comparisons of velocity profiles measured at the inboard forward station with several theoretical profile shapes are shown in Figures 15 to 17 for a variety of test conditions. These profiles are presented in the form of Cole's universal velocity profiles, and include data measured by the Preston tube as the lowest point in each profile. Variations in Mach number, angle of attack, and Reynolds number are shown by Figures 15, 16, and 17, respectively. Since all of these profiles were measured in a generally favorable pressure gradient (although perturbed by the pressure rise through the weak forward shock), they contain very small wake components. Comparisons of the experimental data with the 1/7

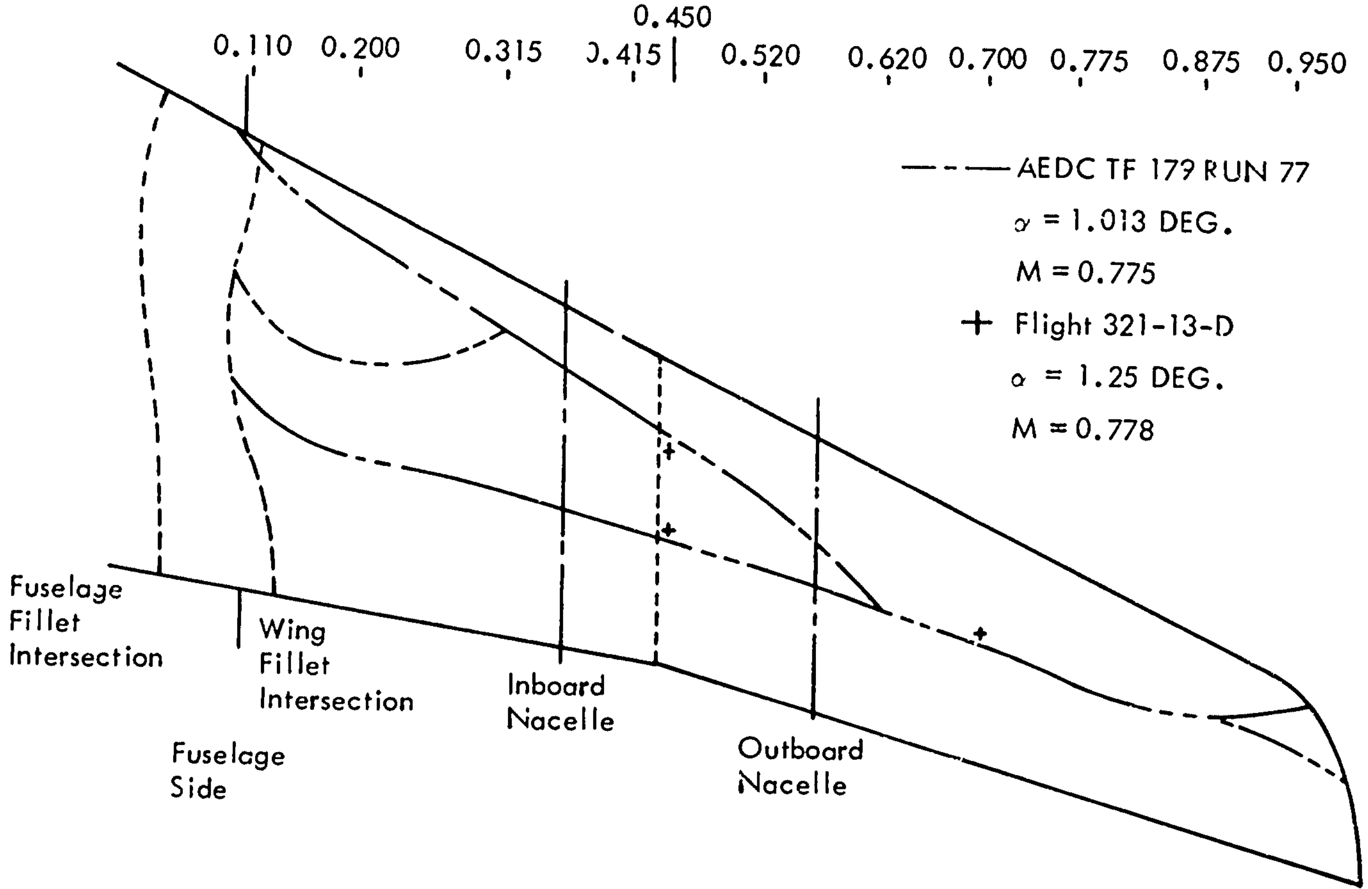

Figure 12. Shock Pattern on the C-5 Wing

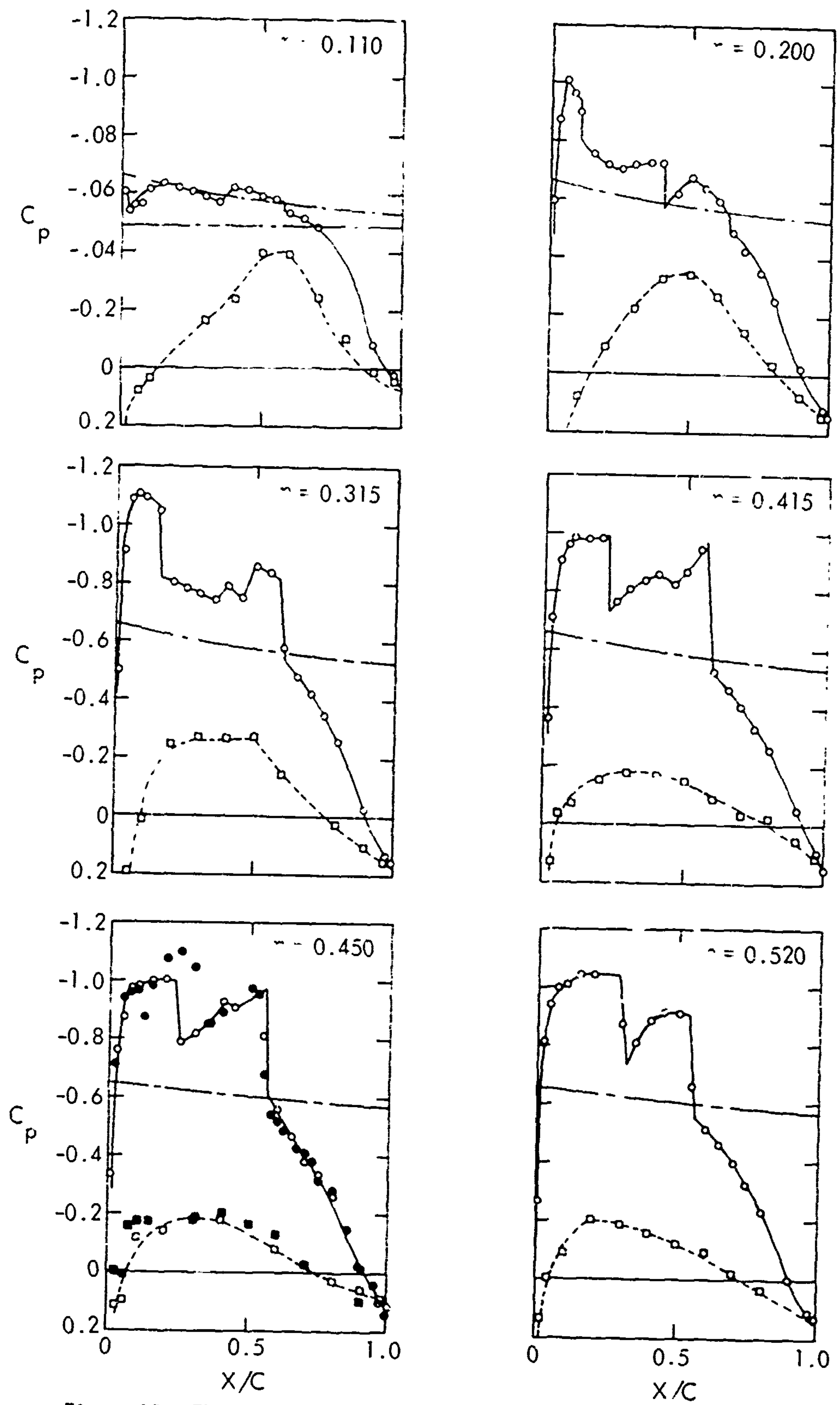

Figure 13. Three-Dimensional C-5 Wing Pressure Distribution Input to the Nash Boundary Layer Program (Sheet 1 of 2)

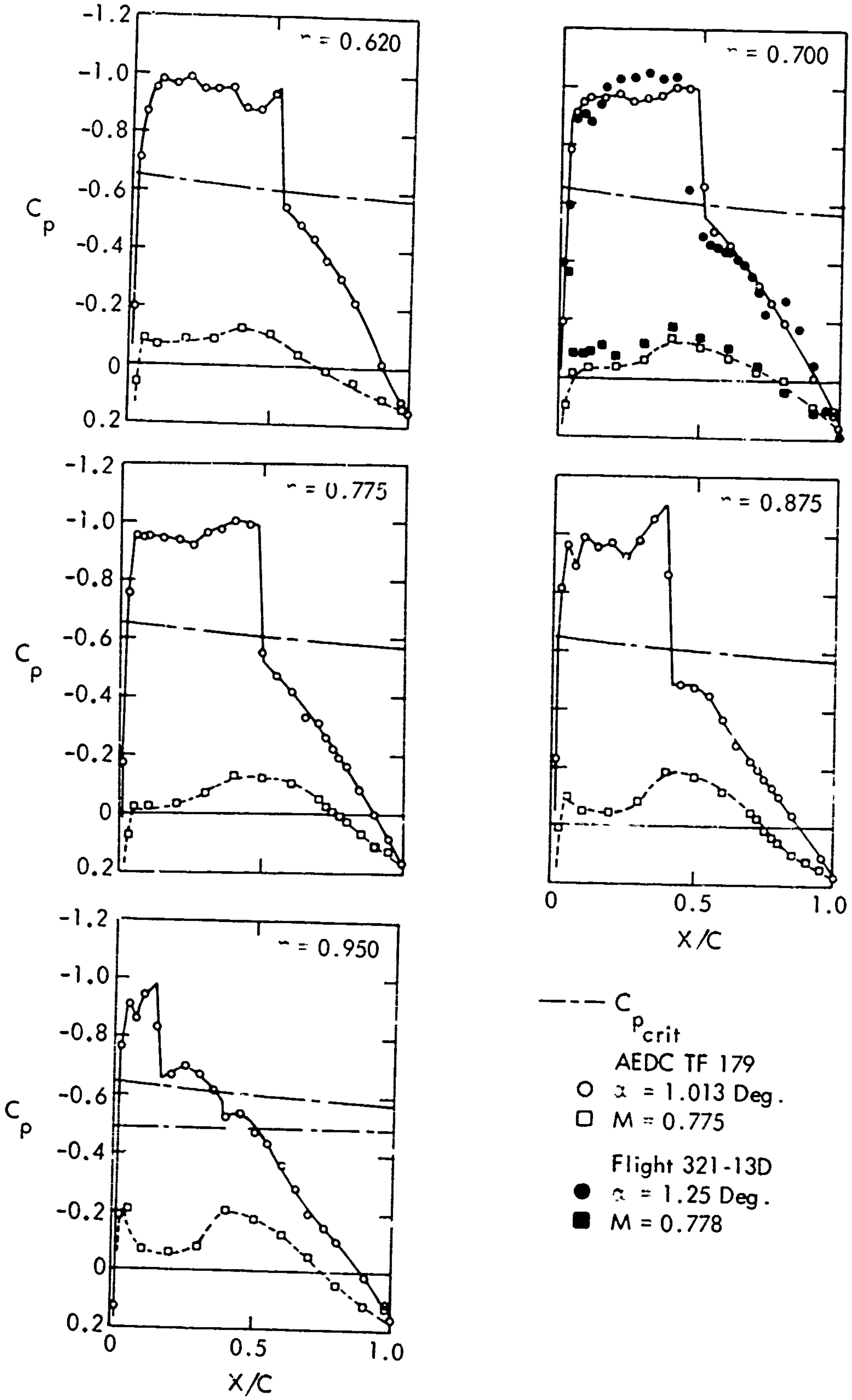

Figure 13. (Sheet 2 of 2)

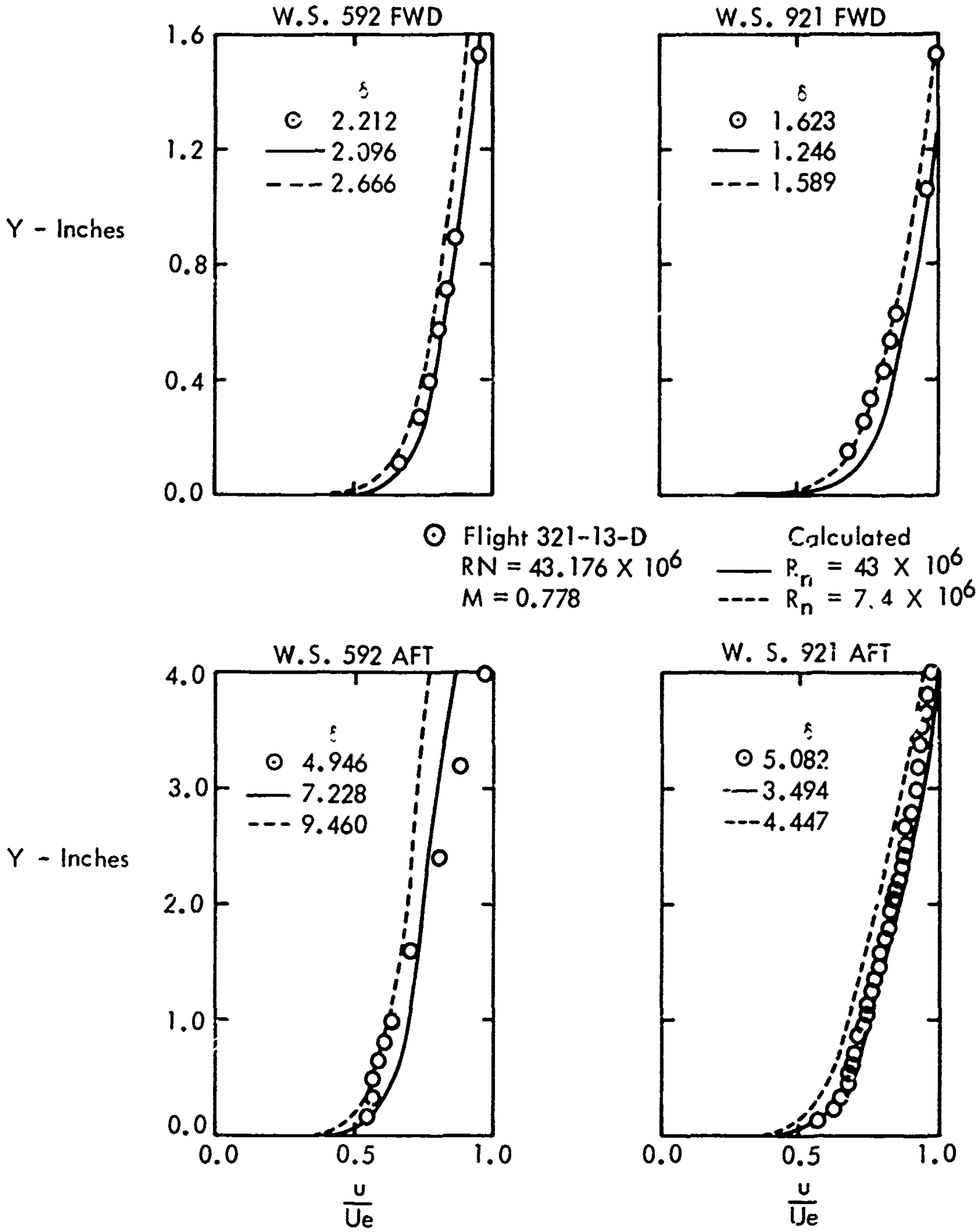

Figure 14. Boundary Layer Profiles Computed By The Nash Method

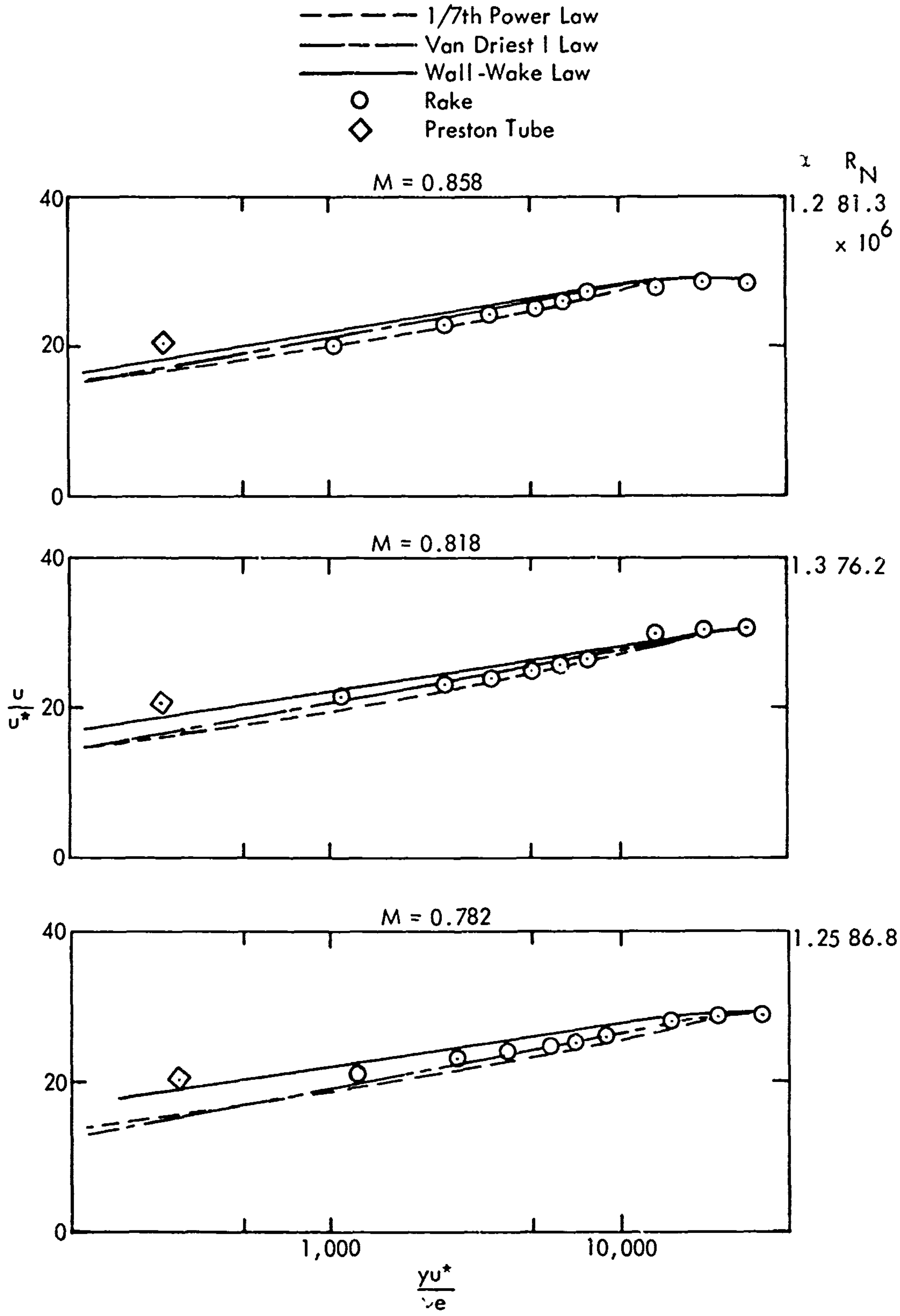

Figure 15. Comparison of Velocity Profiles for Varying Mach Number

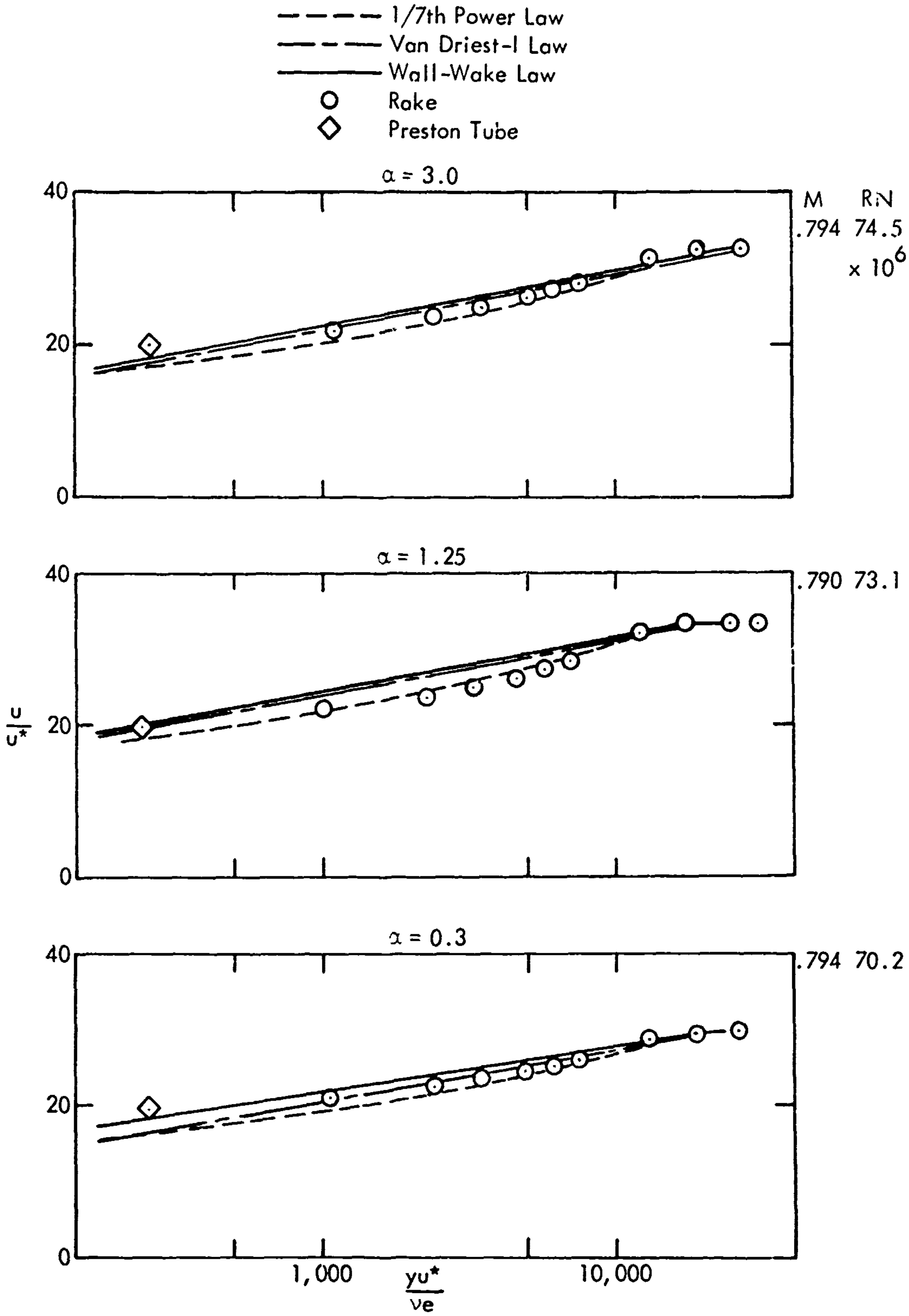

Figure 16. Comparison of Velocity Profiles for Varying Angles of Attack

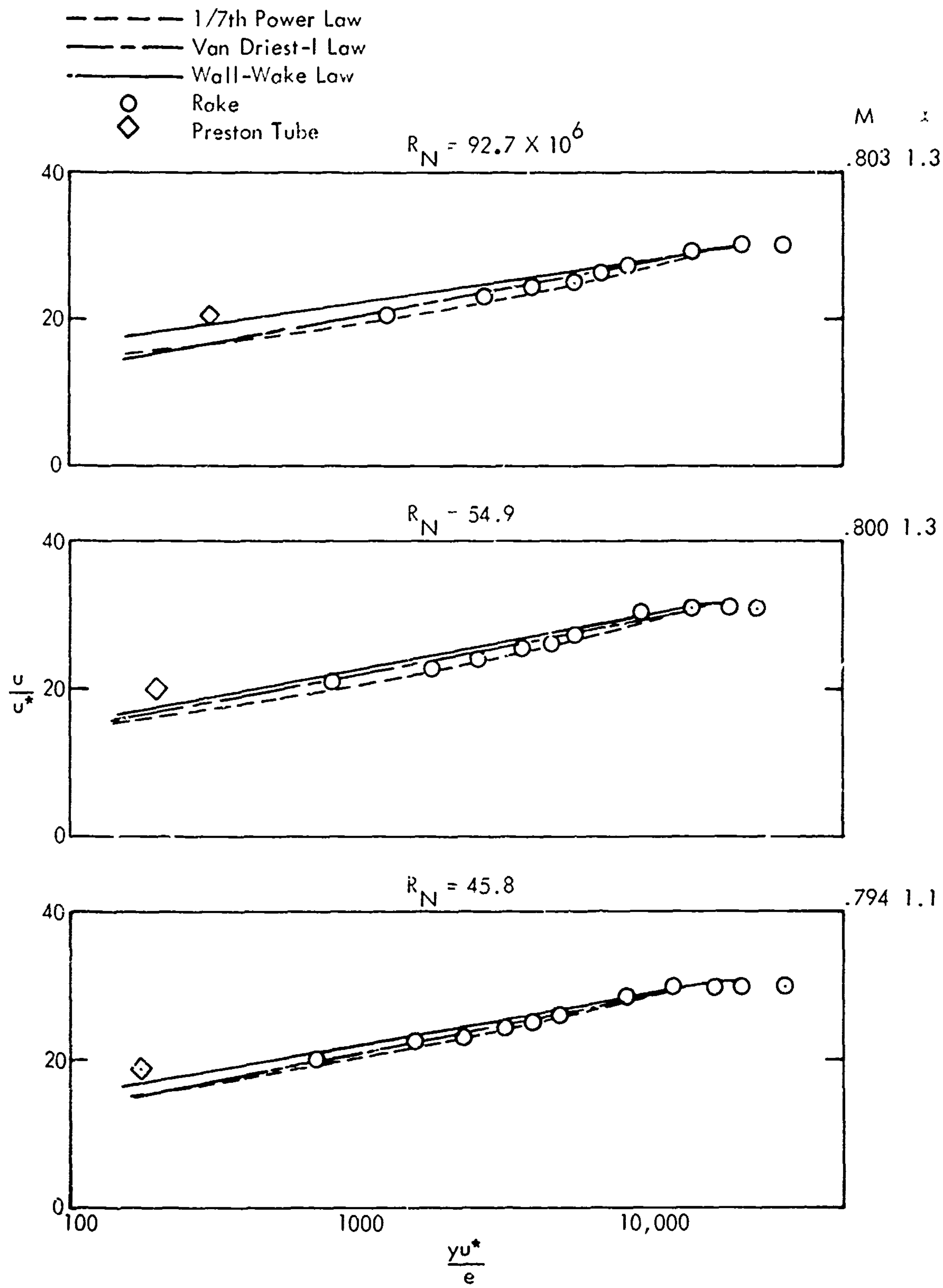

Figure 17. Comparison of Velocity Profiles for Varying Reynolds Numbers

power law, the Van Driest I theory, Reference 8, and Coles wall-wake profile are all fairly good, although generally the 1/7 power law matches the experimental data somewhat better than the other analytical profiles.

Figure 18 shows a comparison of the experimental profiles from the inboard aft rake with the 1/7 power law and the wall-wake profile for several test conditions for which progressively increasing wake components are present. These profiles are shown in both the universal profile form and as plots of u/u_e versus height above the surface. A series of cases for progressively increasing angle of attack was chosen for these comparisons, although small increases in Mach number are also present. The boundary layer is obviously quite close to separation for each of the two higher angle of attack cases as shown by the u/u_e plots. In these cases, the wall-wake profiles obviously must provide the best representation of the boundary layer shapes, and the matching is quite good.

2. INTEGRAL BOUNDARY LAYER PROPERTIES

A number of measured characteristics for each test point from the flight testing are listed in Table I. These data include skin friction coefficient, displacement thickness, momentum thickness, edge Mach number, and shock location, along with test conditions. Figures 19 and 20 present skin friction coefficients, displacement thickness, and momentum thickness values versus Reynolds number for a majority of these points from the forward rakes. The boundary layer thickness values show distinct decreases as the Reynolds number is increased. The edge Mach number, M_e, provided the best parameter for isolating effects other than Reynolds number in these data. This is probably due to the fact that this Mach number is indicative of increases in both favorable pressure gradient and in boundary layer Reynolds number. Trends with Reynolds number are similar in the data from the forward rakes at both spanwise stations. As shown by the upper plots in Figures 19 and 20, no significant trends in variation of skin friction coefficient with test conditions can be identified within the scatter of data available.

For the data measured at the rakes located at 75% chord, behind the shock, the only distinguishable trend demonstrated by the data was a consistent increase in boundary layer thicknesses and a decrease in skin friction coefficient as the Mach number increased (see Figure 21). These trends result, of course, from the increase in pressure rise through the shock as the Mach number increases. The forward rakes are always ahead of the shock and therefore do not experience these effects.

3. CORRELATION WITH TWO- AND THREE-DIMENSIONAL CALCULATIONS

Measured values of skin friction coefficient and boundary layer thickness are shown in Figure 22 compared with data calculated by the Nash three-dimensional method of Reference 7 and the two-dimensional method of Reference 9. In both calculations, the boundary layer transition was assumed to occur at 8% chord. Boundary layer thickness at the forward measuring station matches the three-dimensional theory quite well at both spanwise stations. At the rear rakes, the experimental thickness is higher than calculated outboard and significantly smaller inboard. The profile shape comparisons shown in Figure 14 amplify this comparison. At the outboard station, the experimental profile shape matches

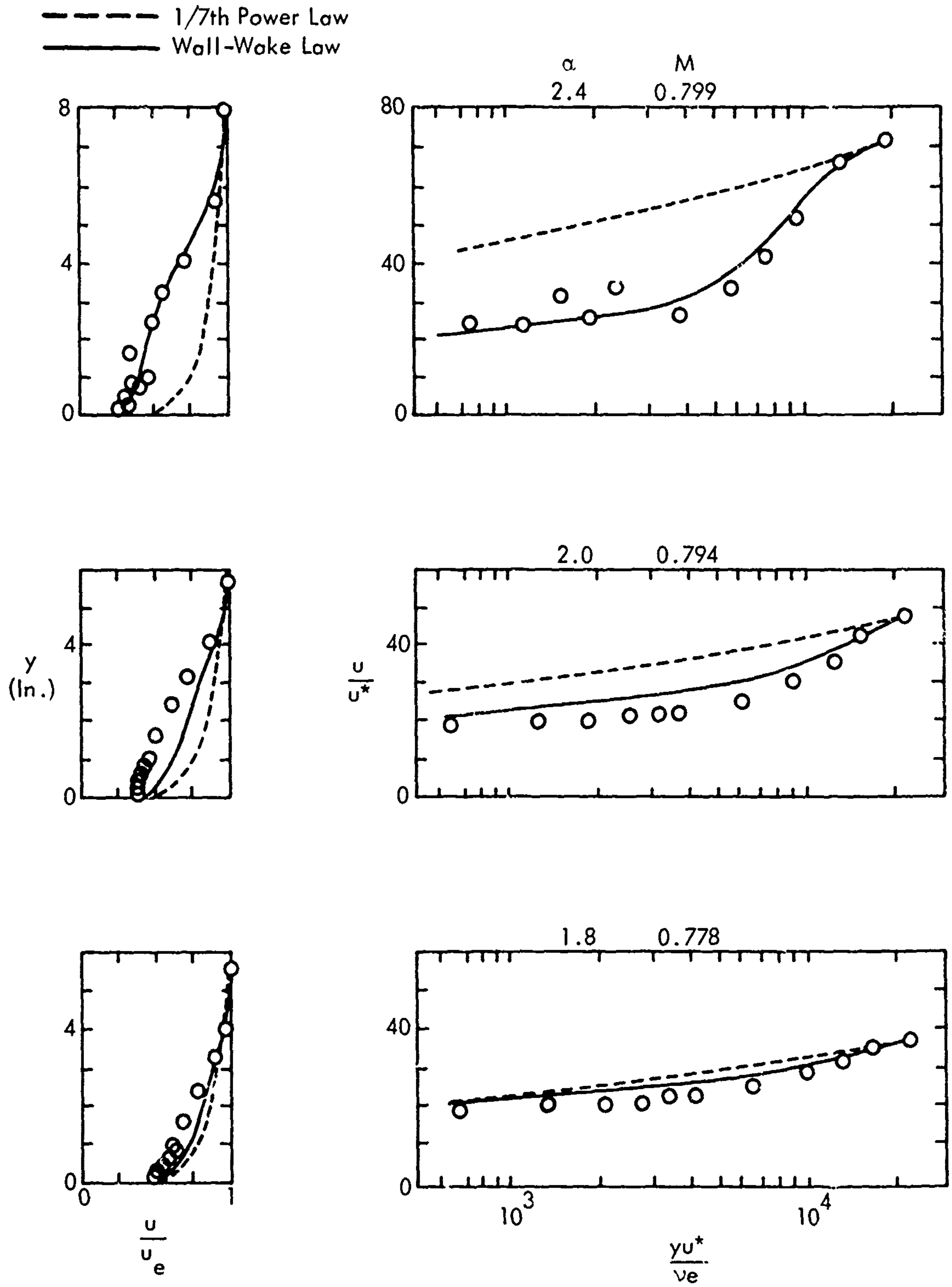

Figure 18. Comparison of the Velocity Profiles for WS 592 Aft with the 1/7th Power Law and Cole's Wall-Wake Law for Varying Deg ees of Separation. Reynolds Number Approximately 50 X 10^6.

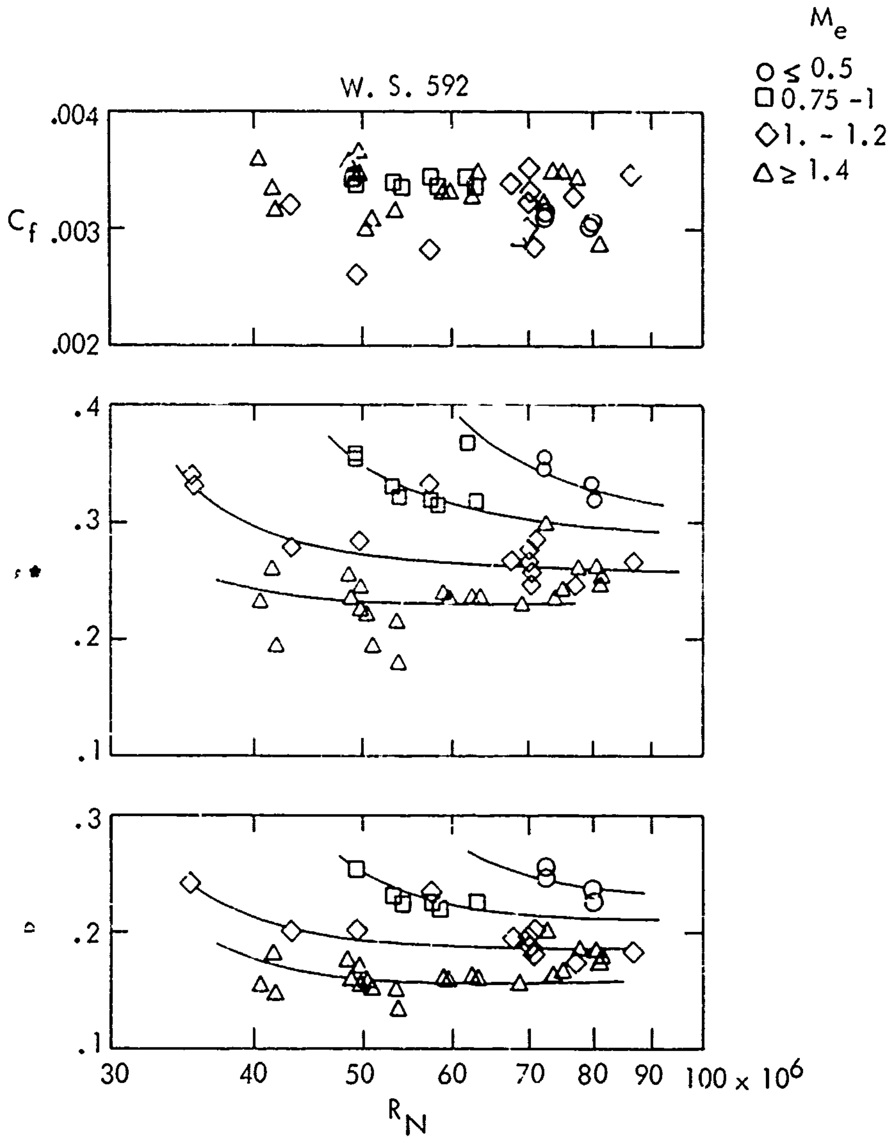

Figure 19. Skin Friction, Displacement Thickness, and Momentum Thickness as a Function of Reynolds Number and Local Mach Number for the Forward Rakes for W.S. 592

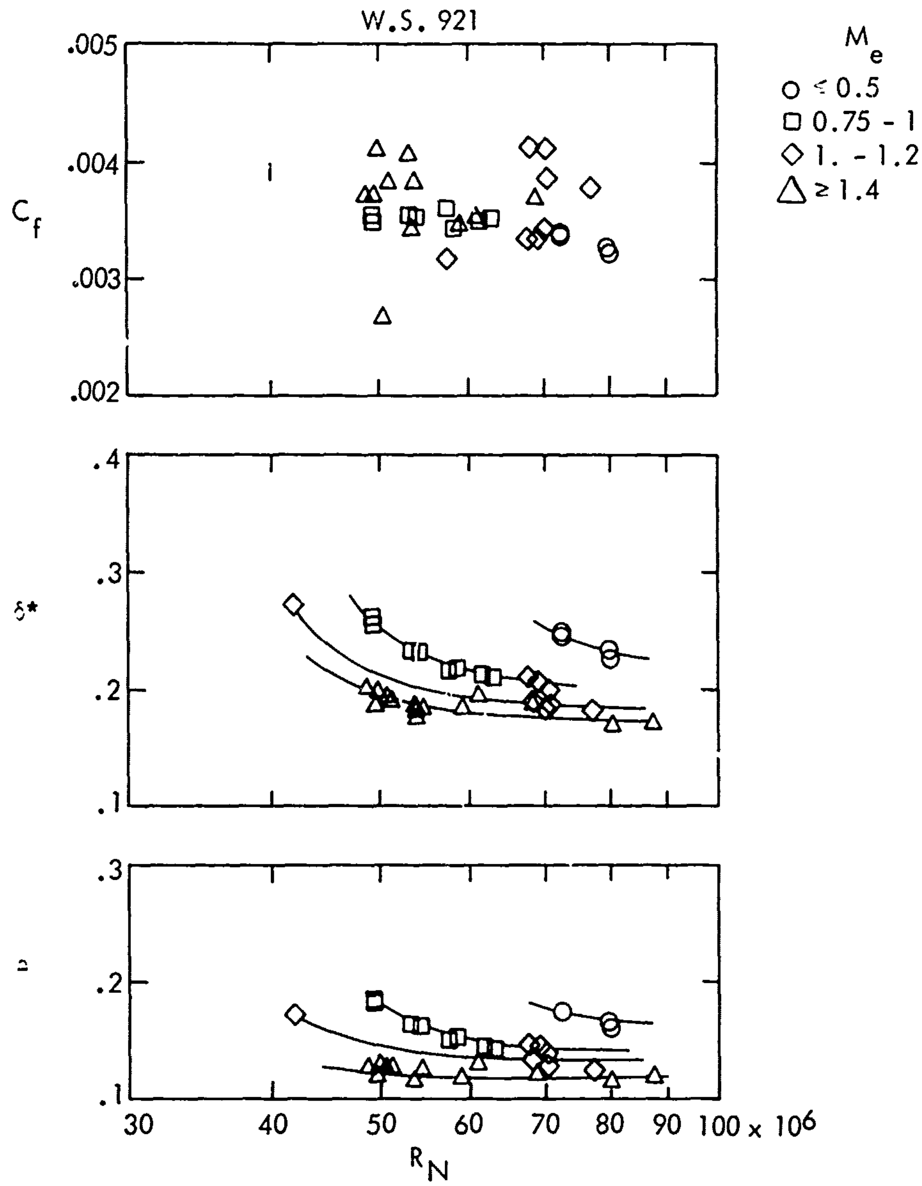

Figure 20. Skin Friction, Displacement Thickness, and Momentum Thickness as Functions of Reynolds Number and Local Mach Number for the Forward Rakes for W.S. 921

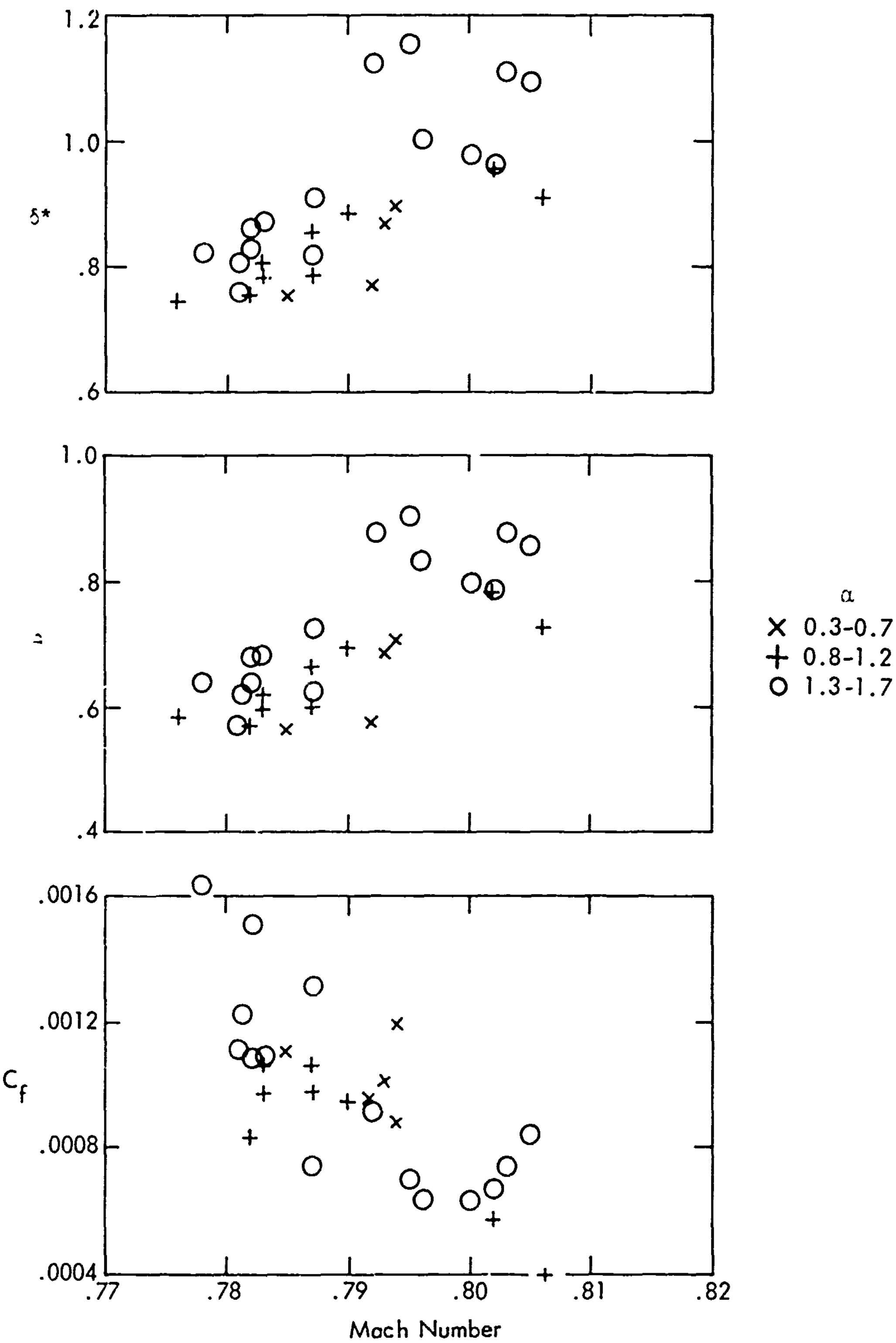

Figure 21. Variation of Boundary Layer Thickness Parameters with Mach Number. x/c = 0.75. Wing Station 592

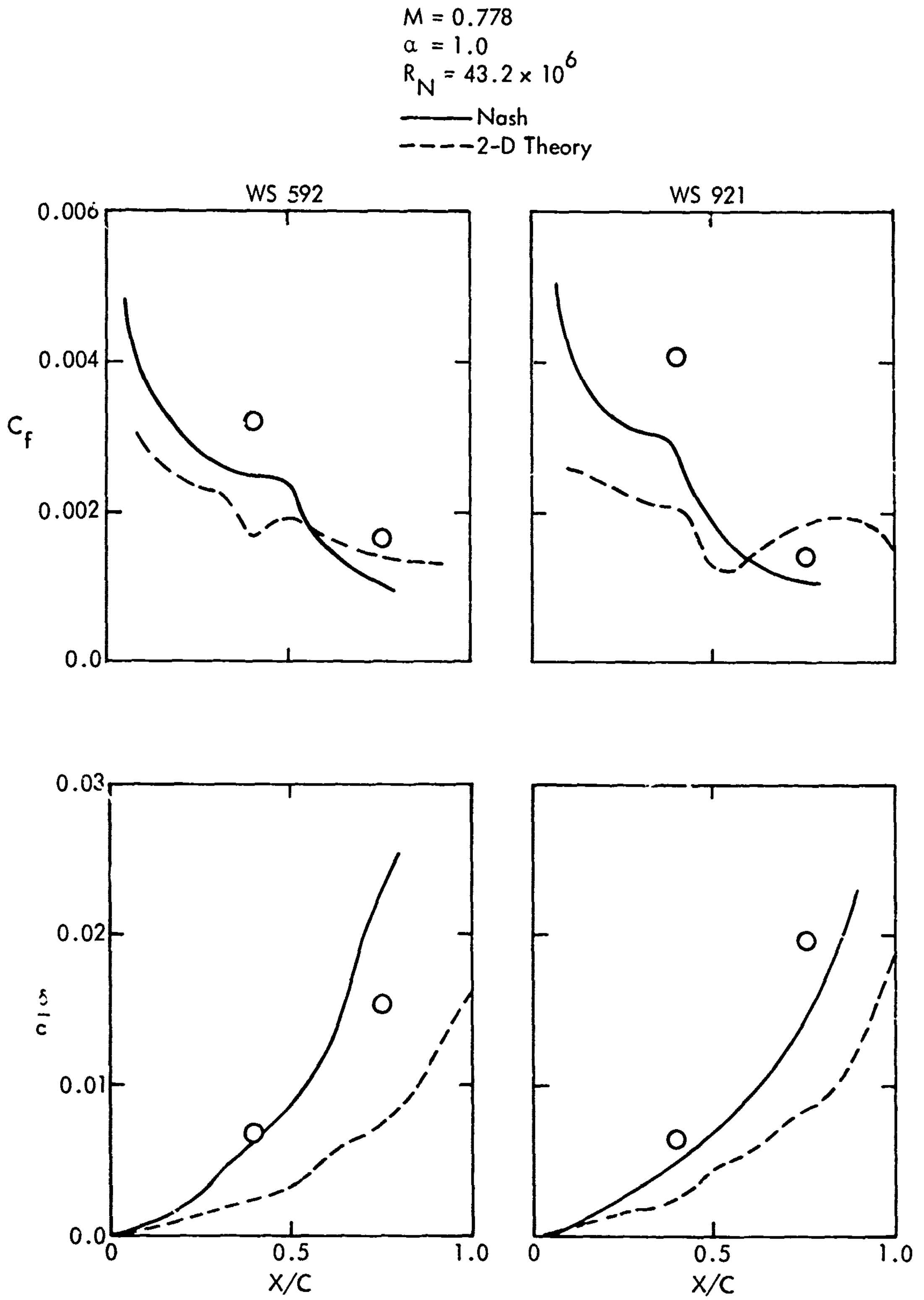

Figure 22. Comparison of Nash's 3-D Theory with 2-D Theory and Flight Test

the calculated shape very well in the lower portion of the boundary layer, but deviates slightly in the direction of a greater thickness in the upper portion. The distortion of the inboard rear profile was discussed previously and is in the direction to produce a low value for the experimental thickness. The two-dimensional thickness calculation always results in a smaller value than the experimental data.

As shown on Figure 22, the experimental skin friction coefficients are generally greater than either the two-dimensional or the three dimensional calculations. While the three-dimensional calculation is obviously better than the two-dimensional, both in discrete values and in the apparent trend with increasing chordwise position, the quantitative correlation is not very good. The surface imperfections discussed in Section II probably form a significant contributor to the higher values of measured skin friction. Experimental values of displacement thickness and momentum thickness are compared with values calculated by the two-dimensional method of reference 9 for variations in Mach number, angle of attack, and Reynolds number, respectively, in Figures 23 to 25. At the forward rakes, the correlation in displacement thickness is very good for all cases. The calculated values of momentum thickness are generally lower than the experimental results. At the rearward rakes, good correlation can hardly be expected because of the strong three-dimensional flow components introduced by the swept normal shocks which are present in the flow ahead of the rear rakes. The two-dimensional method, of course, contains no representation of such flow characteristics, and the approximate correlation shown in some conditions must be considered fortuitous.

Skin friction data resulting from the two-dimensional calculation are shown in Figure 26 correlated against the experimental values. The experimental data at the forward measuring stations show higher skin friction values than predicted, which is compatible with previous comments on the probable effects of surface imperfections. The correlation shown by data from the rear rakes is surprisingly good. It would appear that the validity of using this two-dimensional method for predicting this kind of flow condition should be examined in more detail. In the absence of such an investigation, the correlation shown should be regarded with caution.

4. CORRELATION WITH SKIN FRICTION THEORY

Skin friction coefficients were calculated for the measured local flow conditions at each rake for each test point available, from the Spalding and Chi (Reference 10) and the Van Driest II (Reference 11) theories. Table II contains a partial listing of the calculated and experimental data. Since both of these theoretical methods ignore longitudinal velocity gradients, the correlation of data from the rear rakes with calculated results is so poor as to be meaningless. The difference between calculated and experimental values for the forward rakes is plotted against Mach number in Figures 27 and 28. These differences scatter considerably for both theories, and seem to show a trend from positive values of theory minus experiment at low Mach numbers toward negative values at higher Mach numbers. Although not as well defined, a trend toward smaller scatter at high Mach numbers might also be inferred from these data. No consistent trend with Reynolds number could be extracted from these data.

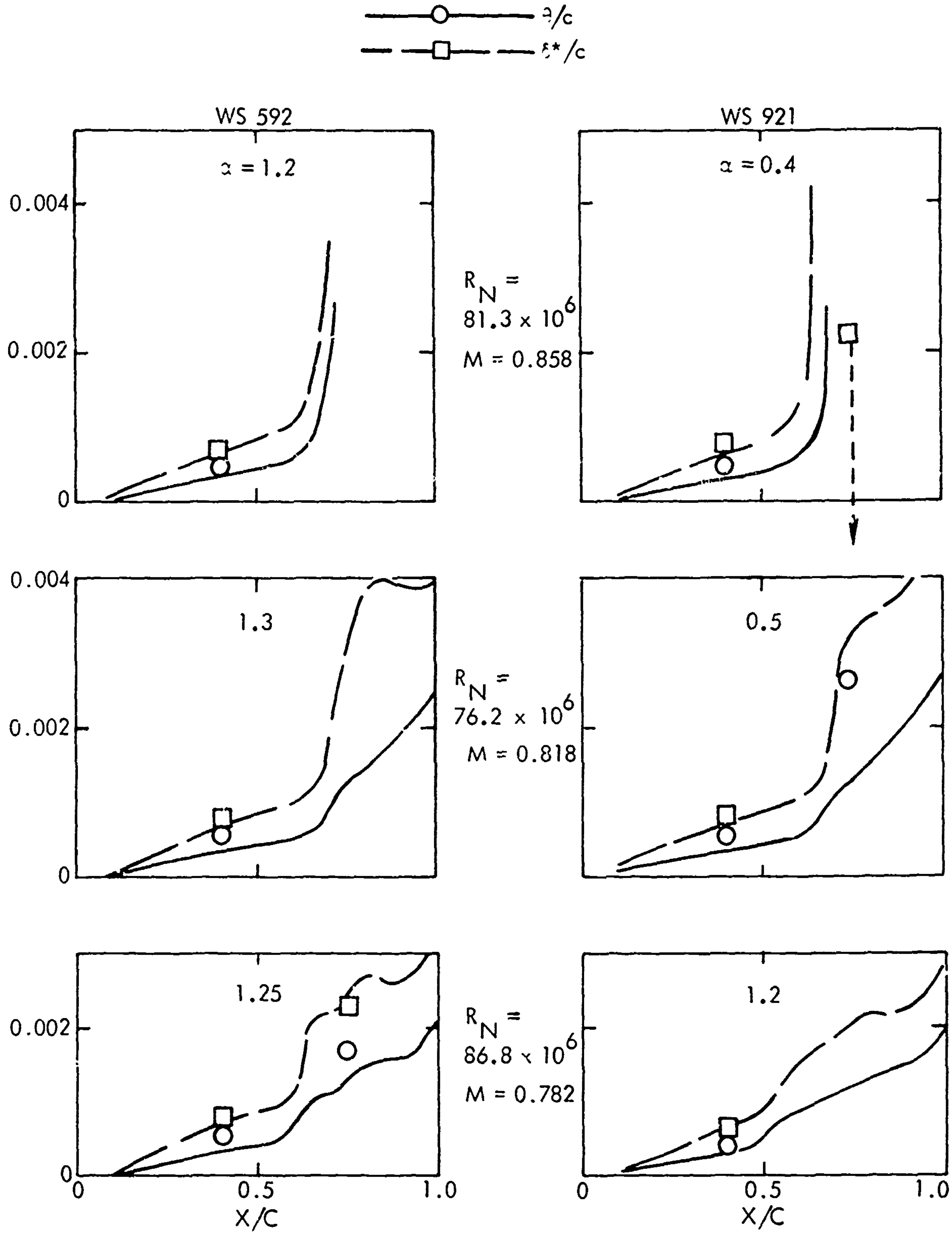

Figure 23. Comparison of Momentum and Displacement Thicknesses for 2-D Theory (Reference 9) and Flight Test

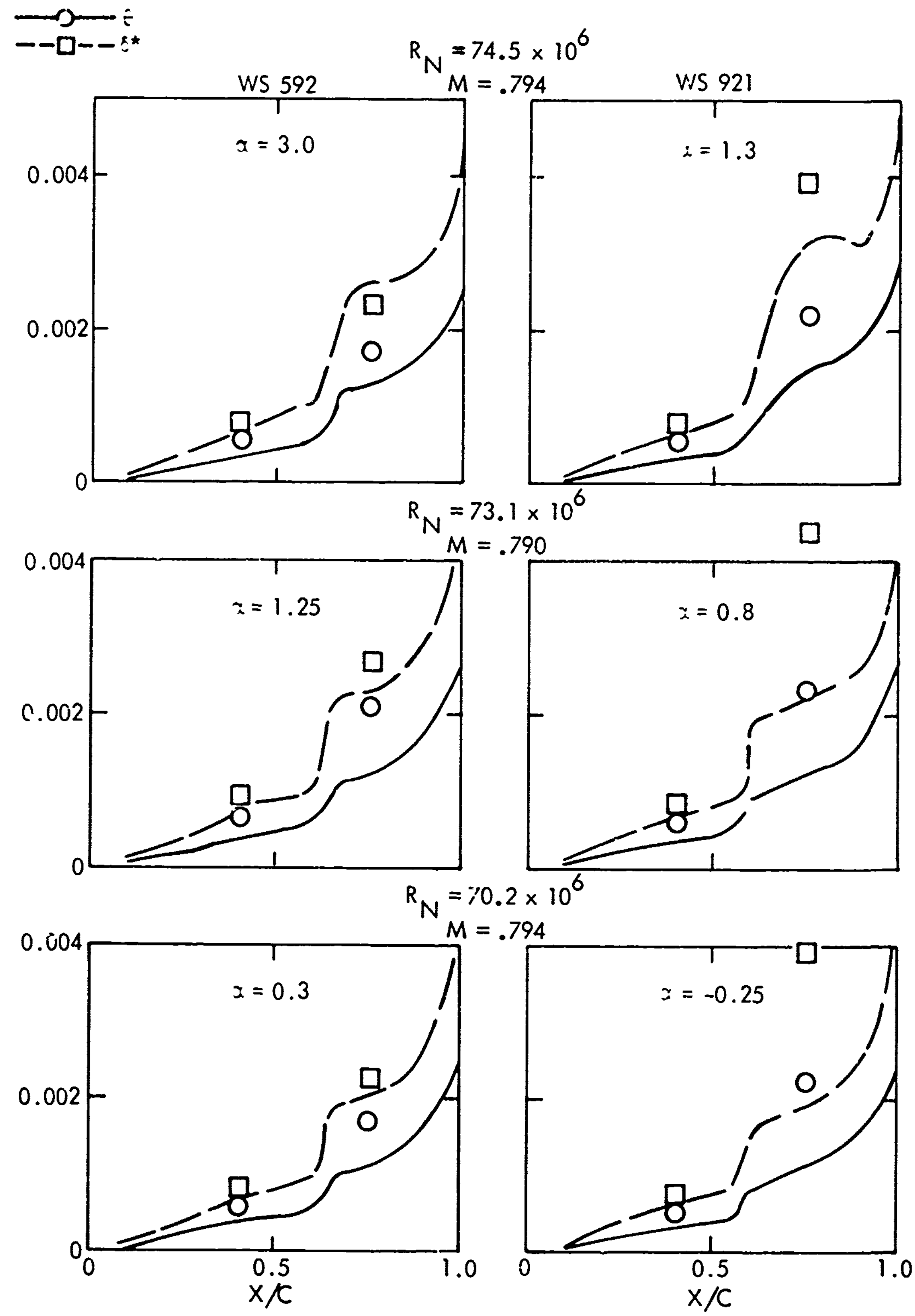

Figure 24. Comparison of Momentum and Displacement Thicknesses for 2-D Theory (Reference 9) and Flight Test

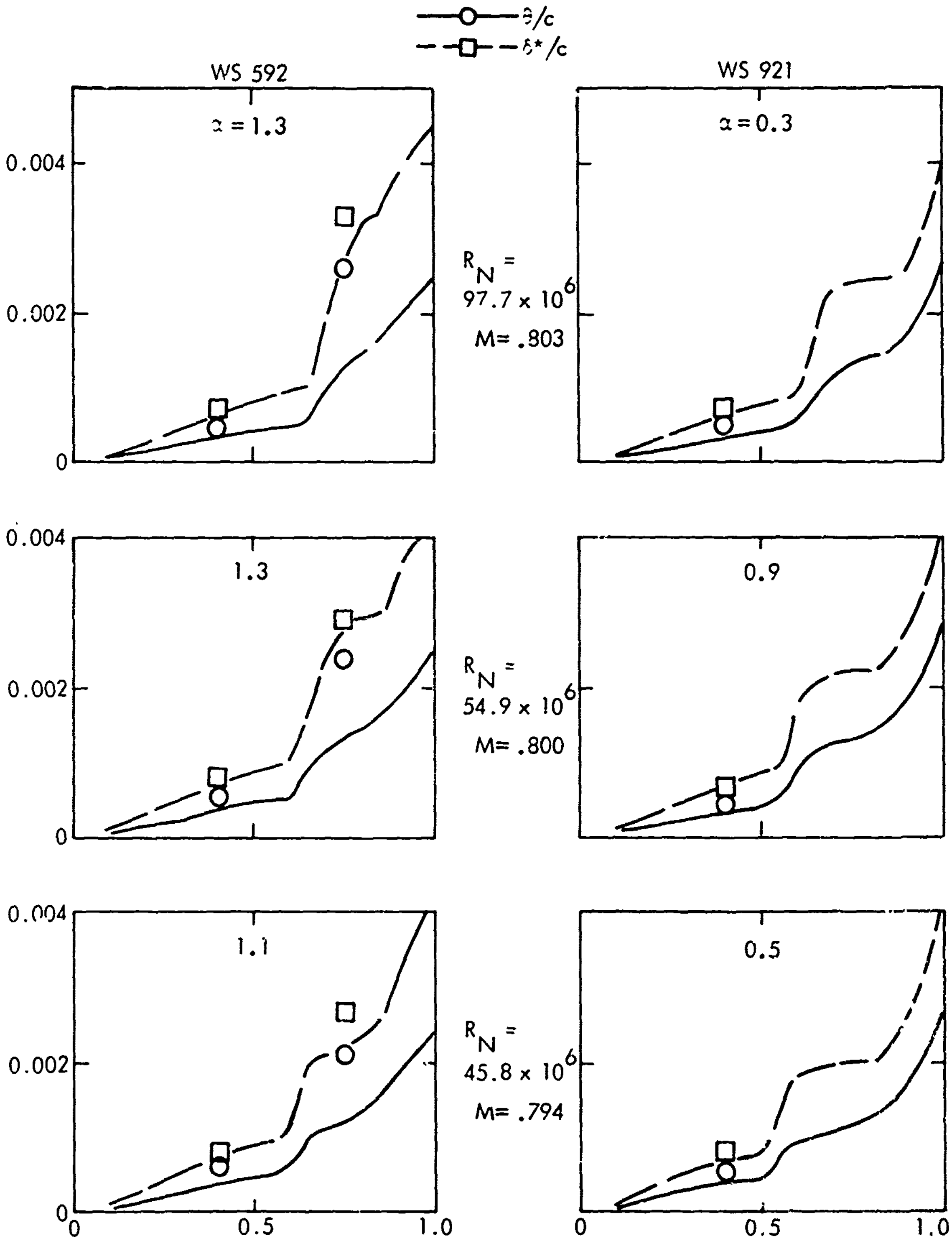

Figure 25. Comparison of Momentum and Displacement Thicknesses for 2-D Theory (Reference 9) and Flight Test

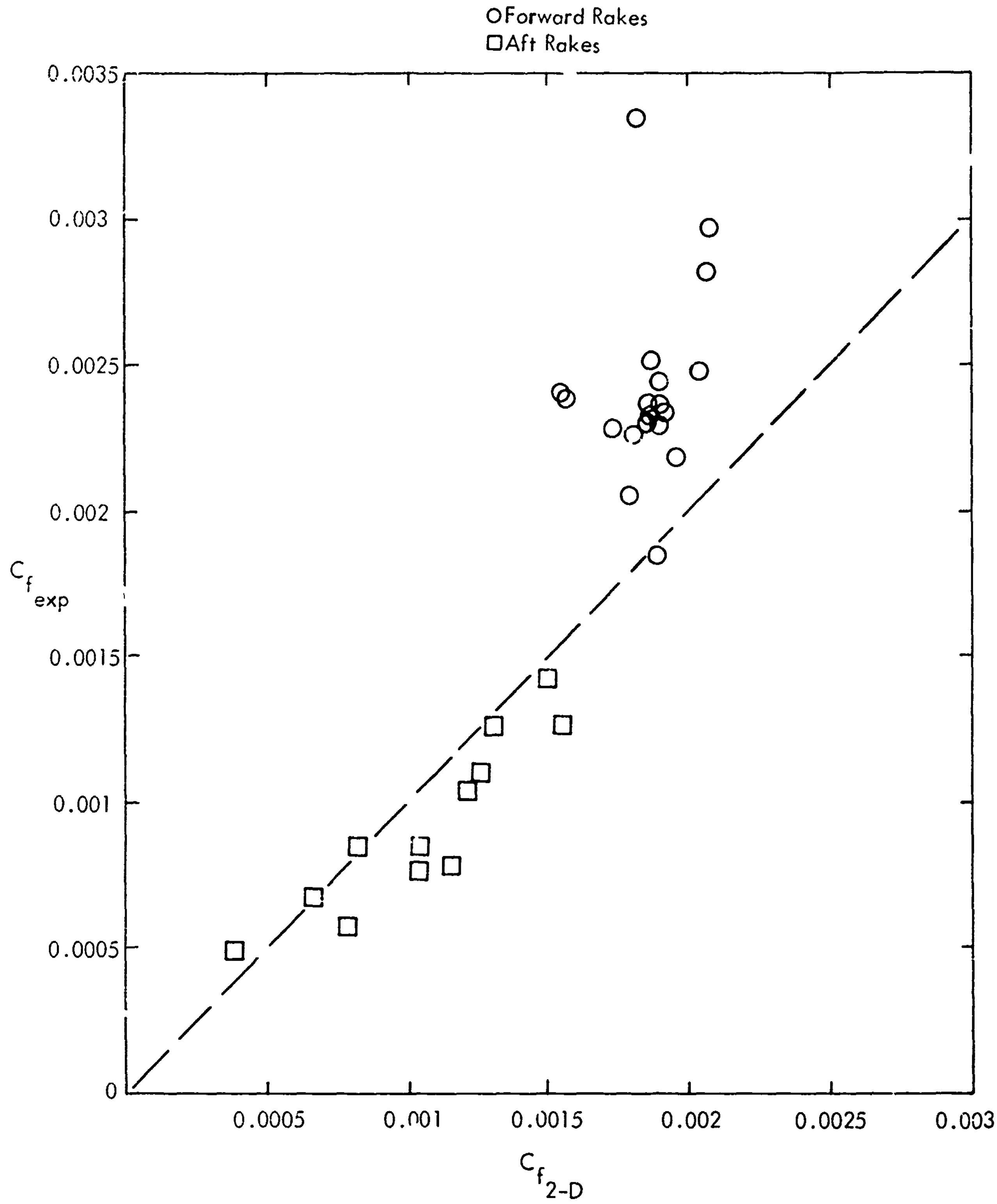

Figure 26. Comparison of Skin Friction from 2-D Theory (Reference 9) and Flight Test

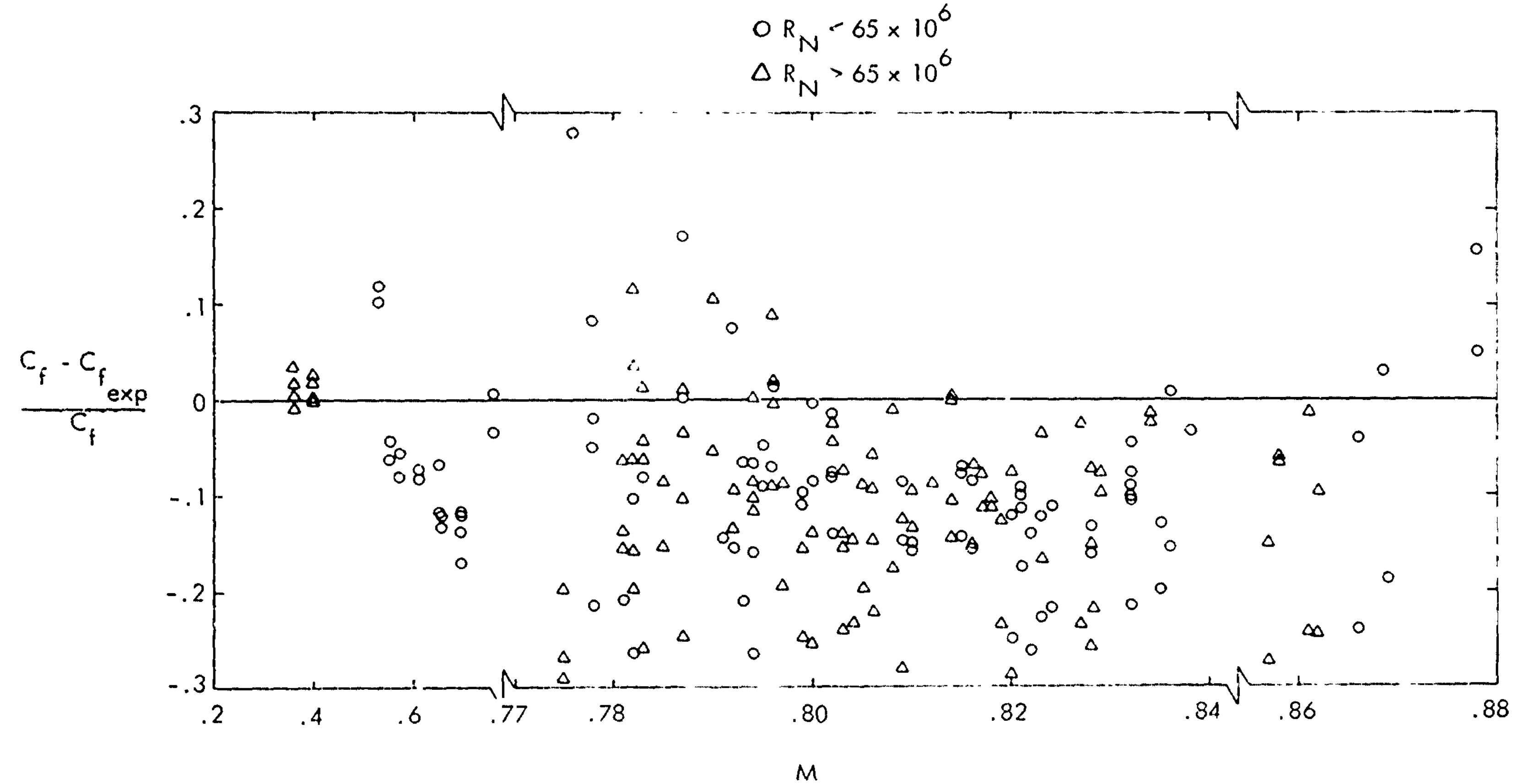

Figure 27. Comparison of the Spalding-Chi Skin Friction Theory with Flight Test Data

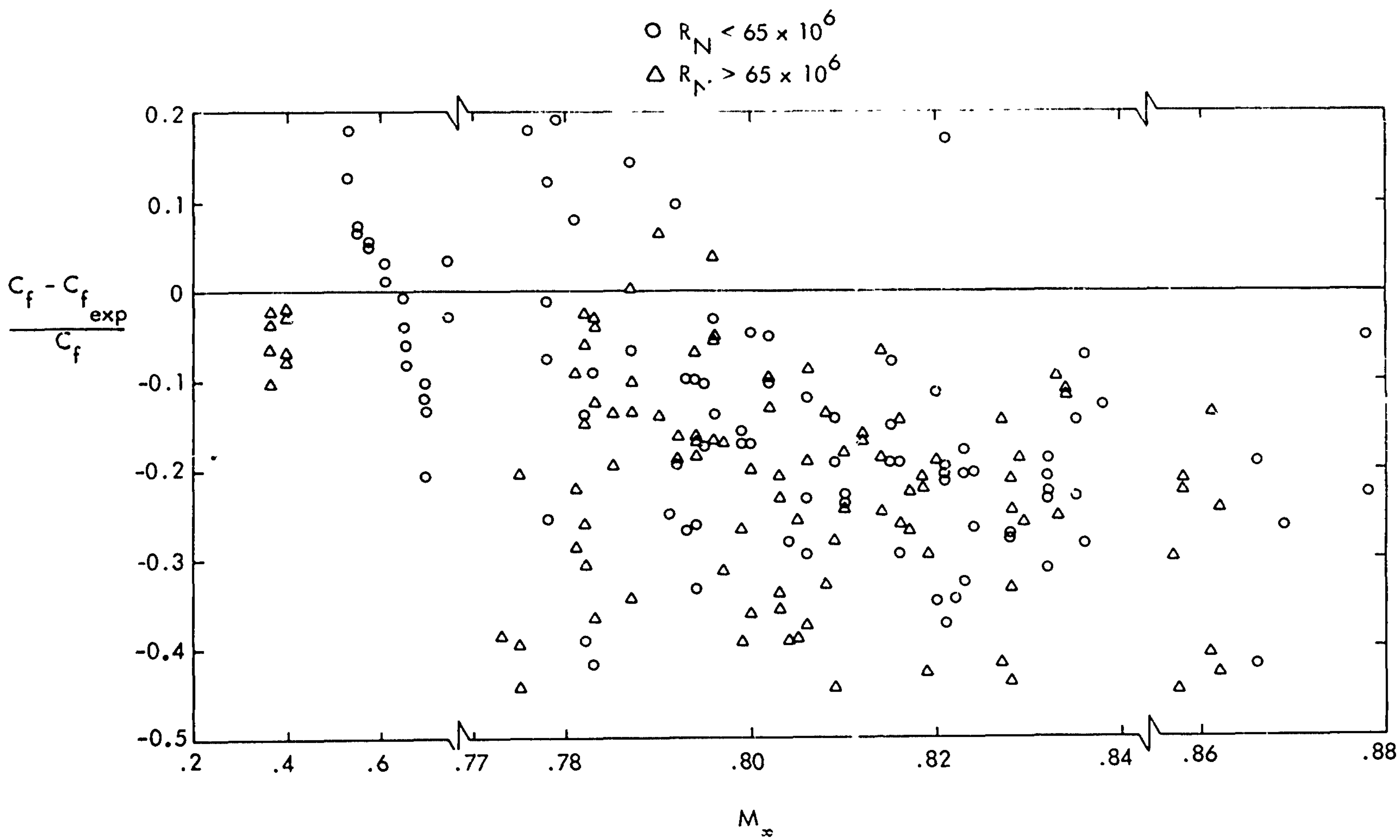

Figure 28. Compurison of the Van Driest II Skin Friction Theory with Flight Test Data

An examination of the data at various angles of attack, on the other hand, shows a reasonably well defined trend toward lower skin friction values at higher angles of attack Figure 29 shows this variation for the experimental data in a narrow band of Mach number (0.798 ± 0.005). Plots of the normalized difference between theory and experiment, also shown in Figure 29 for both the Spalding-Chi and the Van Driest II theories, reflect this trend, but the scatter remaining in the data is sufficiently large that an accounting for angle of attack variations will not change any conclusion to be drawn from Figures 27 and 28.

5. TEMPERATURE AND DENSITY PROFILES

Peak values of local Mach number occurring in the data considered here are of the order of 1.3 to 1.4. Temperature changes through the boundary layer are, therefore, not large. Temperature profiles measured for several flight Mach numbers are shown in Figure 30, along with values calculated from the well-known Crocco relation for an adiabatic wall:

$$\frac{U}{U_e} = \frac{T_o - T_w}{T_{o_e} - T_w}$$

The measured data follow the calculated curves with only a small discrepancy for one profile. The Crocco theory and the measured temperatures were used to calculate the density profile through the boundary layer . (The static pressure is assumed constant.) These profiles are compared in Figure 31 and also show near agreement.

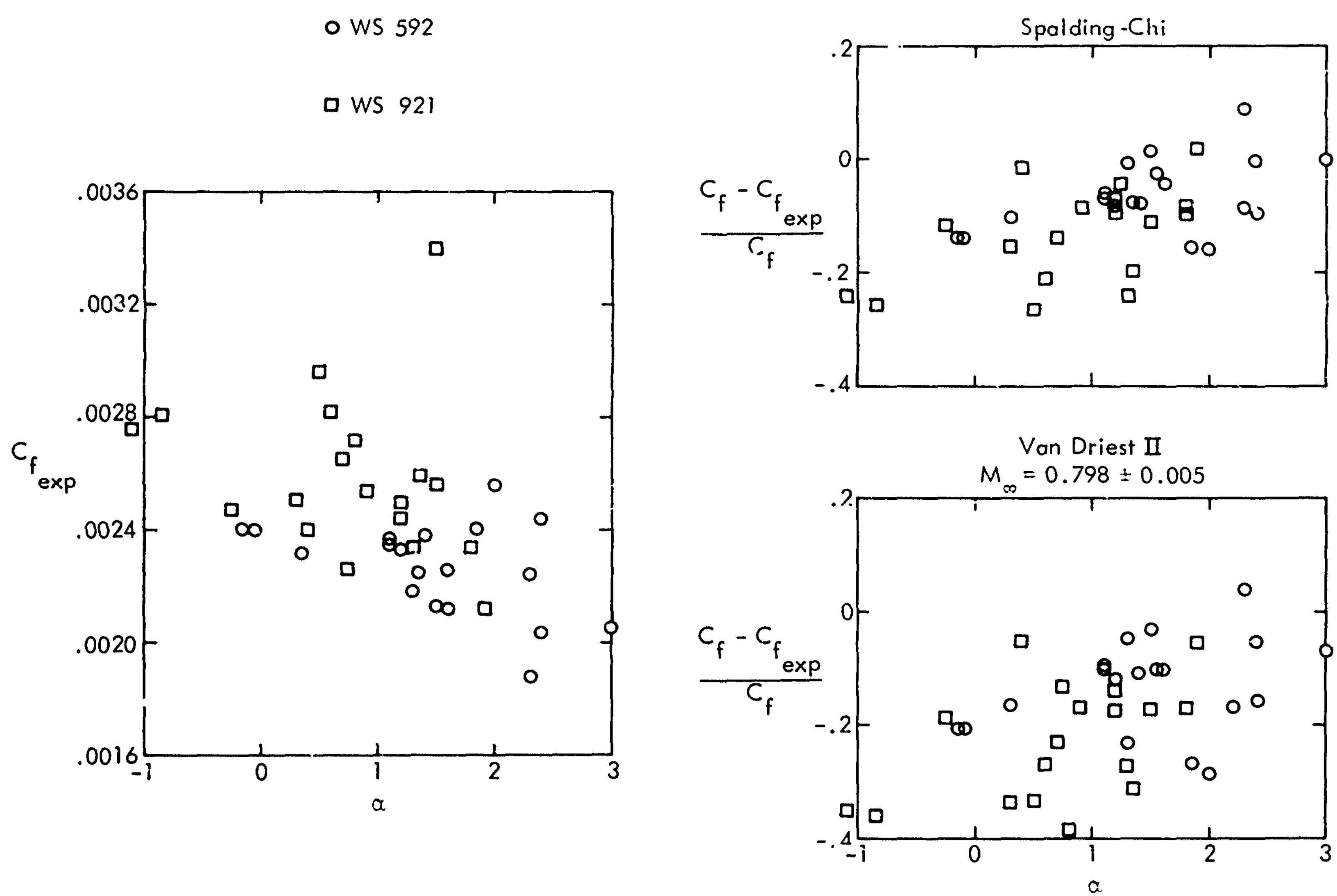

Figure 29. Variation of Skin Friction with Angle of Attack for Mach = 0.798 ± 0.005

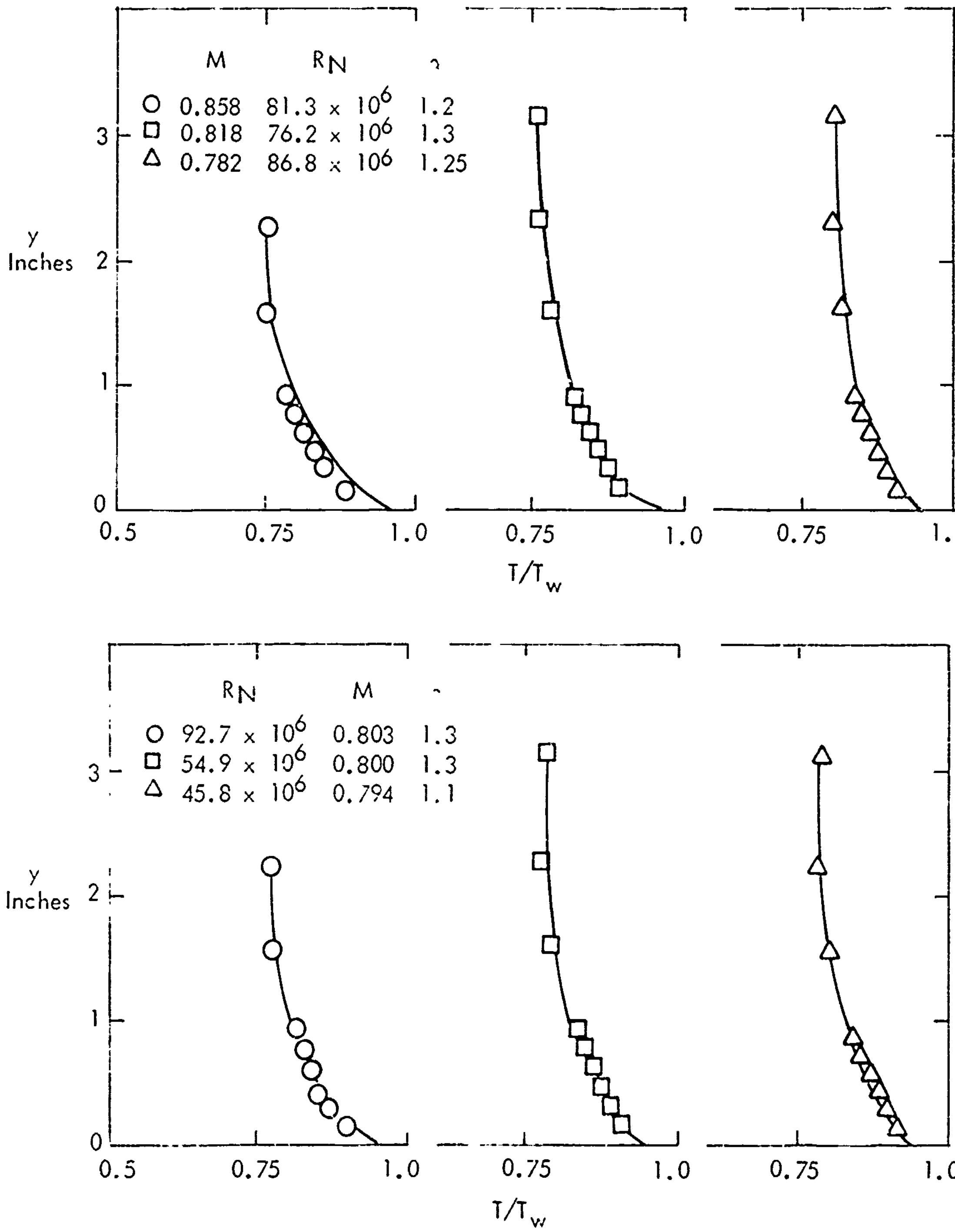

Figure 30. Comparison of Static Temperature Profiles with Crocco's Theory

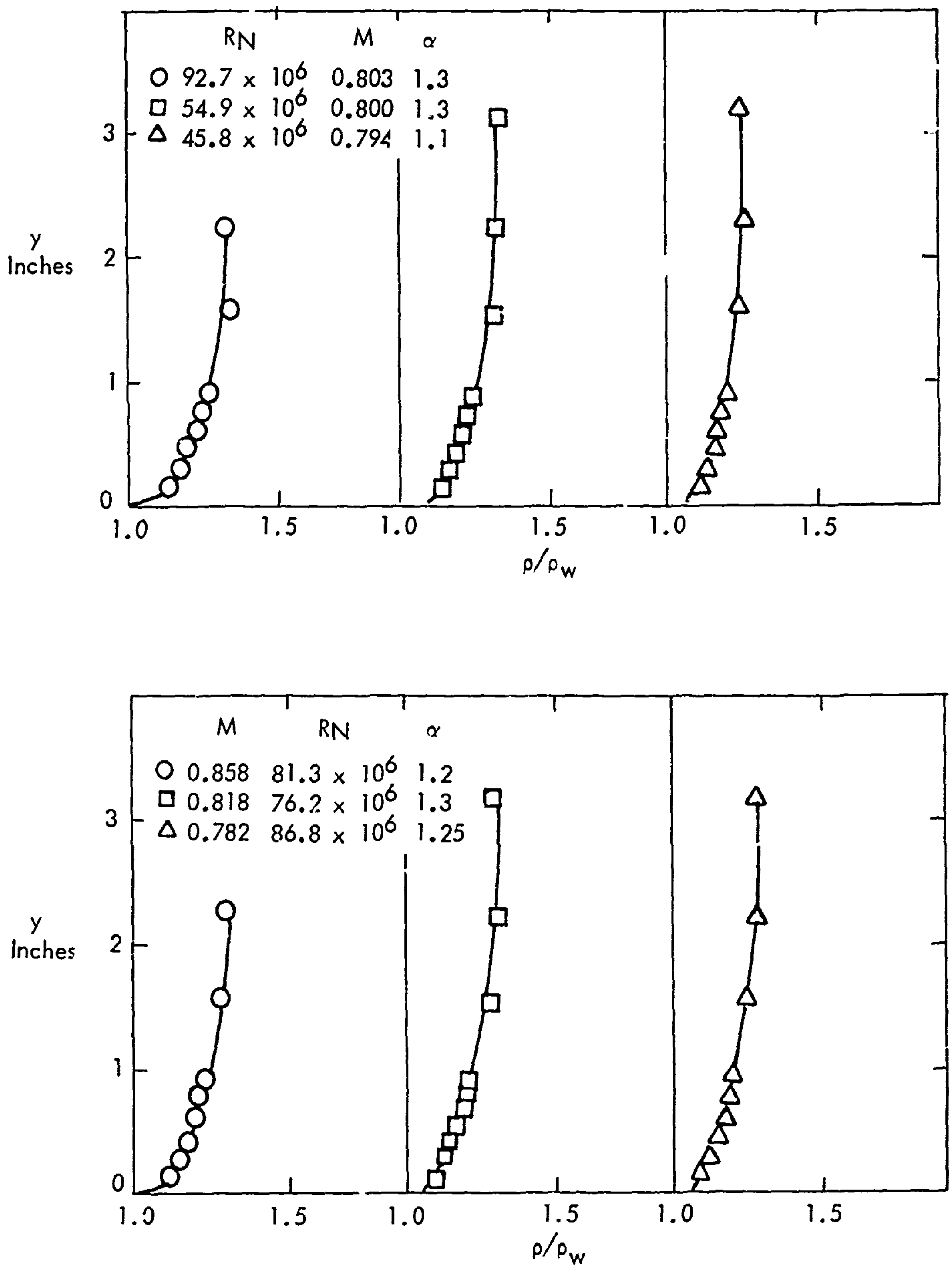

Figure 31. Comparison of Density Profiles with Crocco's Theory

SECTION V

ANALYSIS OF SCALE EFFECTS ON SHOCK-INDUCED SEPARATION

As discussed in Section I, previous investigations have shown that the outstanding effects of shock-induced separation on wing load distributions at transonic speeds have been manifested as changes in the location of the normal shock which terminates the local supersonic flow region on the wing upper surface. Data obtained in this investigation which relate to this phenomenon and the scale effects indicated by these data will be reviewed in this section.

1. VARIATIONS IN SHOCK LOCATION

Although the terminal shock in a transonic wing flow field functions as a normal shock (since it provides the transition from supersonic to subsonic flow), the wing surface pressure distribution does not display the instantaneous pressure rise characteristic of a mathematical normal shock. Therefore, to provide a quantitative entity for comparisons of shock location, the definition illustrated in the following sketch has been adopted for shock location.

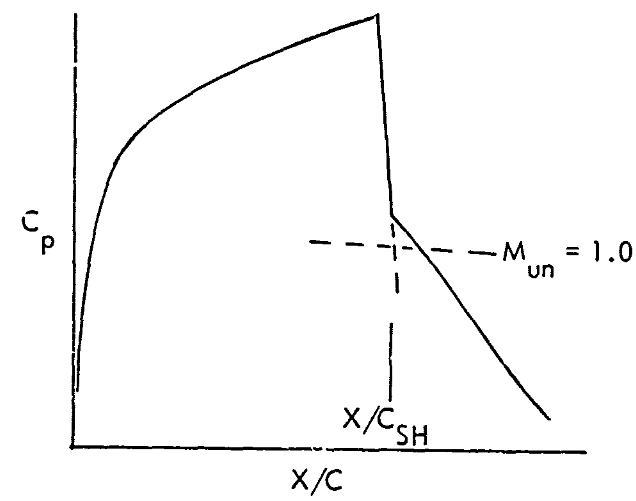

A straight line is fitted to the shock pressure rise. The intersection of this straight line with the line representing the local values of critical pressure coefficient for the flow normal to the local element lines of the wing is defined as the shock location.

Figures 32 and 33 show the variation of measured shock locations with Mach number and Reynolds number for several angles of attack. To establish the shock location values shown at fixed angles of attack, the variation of shock location with angle of attack was first determined from the mass of data available, and all data within a narrow band of angles of attack were corrected to account for the difference from the nominal angles

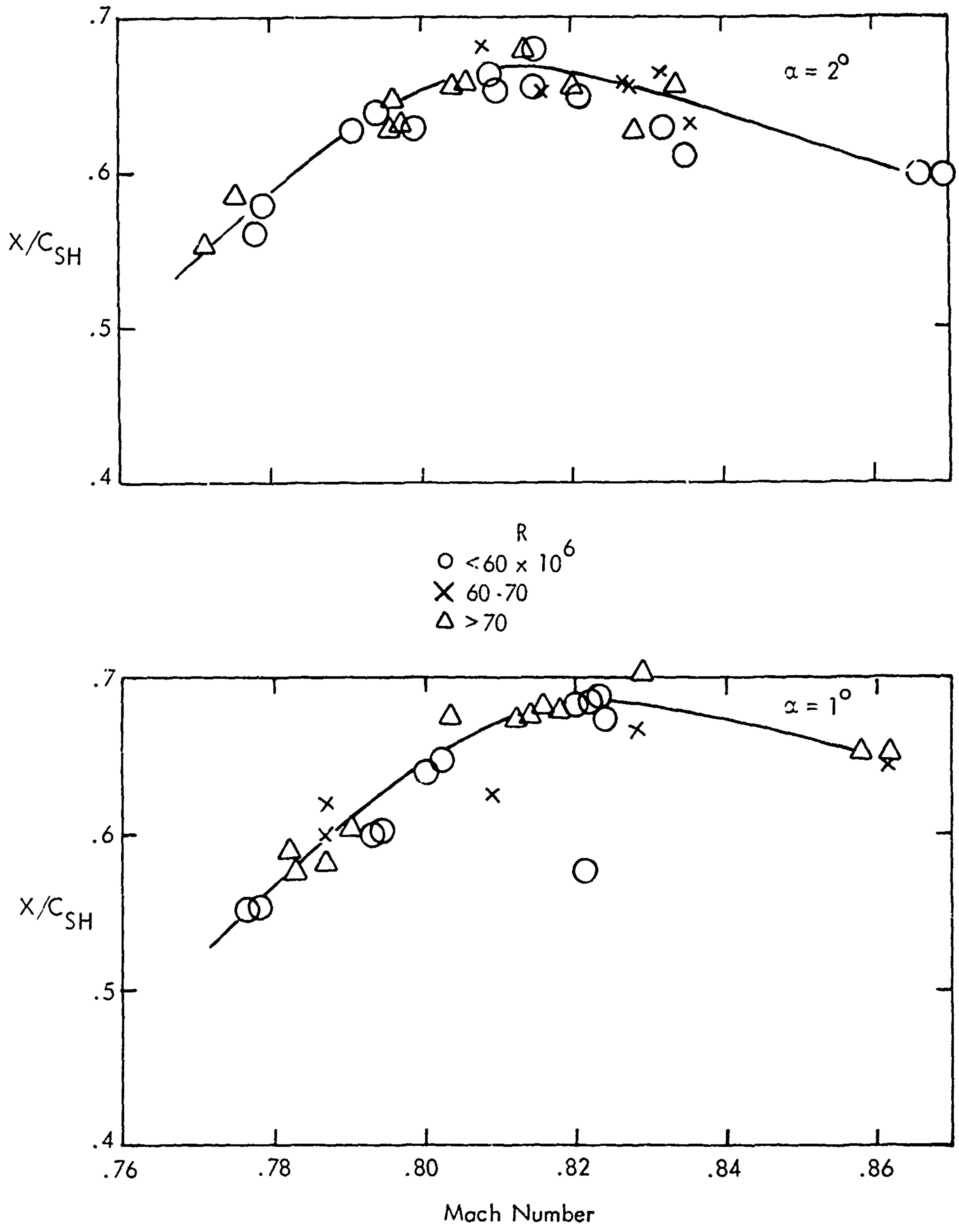

Figure 32. Variation of Shock Location with Mach Number, Reynolds Number, and Angle of Attack. Wing Station 592

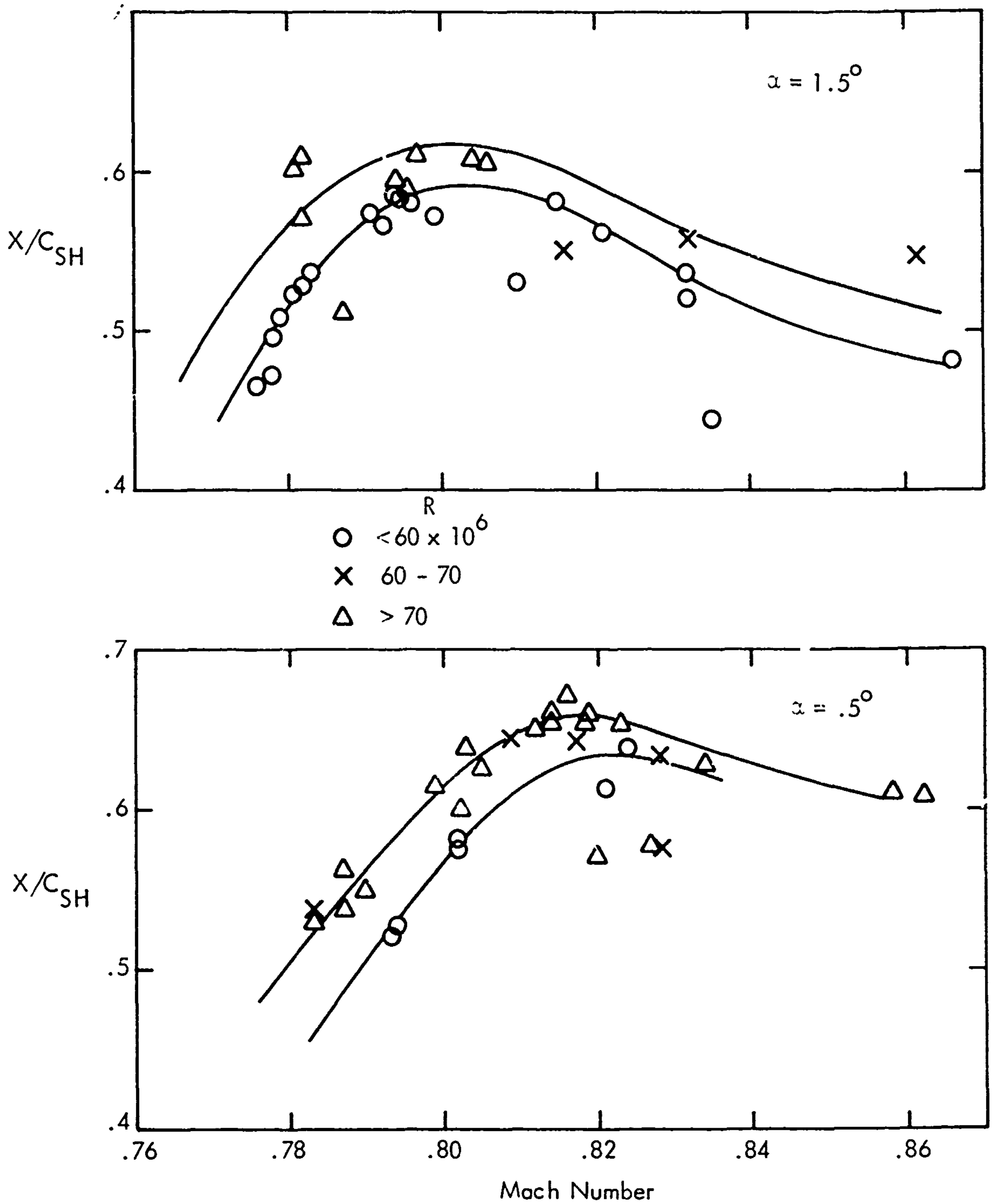

Figure 33. Variation of Shock Location with Mach Number, Reynolds Number, and Angle of Attack. Wing Station 921

selected. The data shown in Figures 32 and 33 include all test points within ±0.3 degree from the nominal angles.

For the data measured at wing station 592, Figure 32, some scatter is shown by the measured data, but no consistent variation of shock location with Reynolds number can be discerned. The shock location moves aft as the Mach number is increased from the minimum values tested to a Mach number of approximately 0.82, following which a small forward movement occurs.

At wing station 921, Figure 33, a similar trend with Mach number is shown, and a small but distinct aft movement of the shock (approximately 5% C) with increase in Reynolds number is observed. The reason for this difference is not readily apparent. A number of factors contribute to making conditions at the outboard station different from those farther inboard.

- Only a single shock is apparent in the flow on the outboard wing, while the inboard wing experiences an additional sharp compressive disturbance forward of the terminal shock.

- Flow disturbances from the pylons and nacelles are stronger for the inboard station.

- Due to aeroelastic twist of the wing structure, the effective angle of attack is always higher inboard than outboard.

Because of these, and possibly other, differences in flow phenomena, it is not certain that the differences in shock location shown for different Reynolds numbers in Figure 33 are actually scale-effect differences.

Figure 34 shows the faired curves of shock location versus Mach number for $\alpha = 1.5^{\circ}$ from figure 33, along with similar data from previous wind tunnel testing of a C-5A model (Reference 5) and trailing-edge pressure coefficients from both the wind tunnel and flight tests. At low Mach numbers, the high Reynolds number, flight measured shock locations tend to agree with the wind tunnel values better than the lower flight Reynolds number data. This fact seems to confirm the conclusion that differences in flight shock locations cannot be attributed to Reynolds number differences.

The direct correlation of shock location change and trailing-edge pressure recovery is readily apparent in Figure 34. The flight data, because of higher Reynolds number, show more positive values of the trailing-edge pressure coefficient than the wind tunnel results; and the initiation of separation, as indicated by a deterioration in pressure recovery, is delayed to a higher Mach number. As the Mach number is increased from the lower values shown, the trailing-edge pressure coefficient first remains essentially constant at a value of approximately 0.16 for the wind tunnel case and 0.23 for the flight results. In this range of Mach numbers, the shock first moves aft as a nearly linear function of Mach number, then decreases slope, reaching a peak value at a Mach number of 0.79 at the wind tunnel Reynolds number and 0.8 at the flight Reynolds number. The Mach numbers for these peak values correlate closely with the Mach number at which significant trailing-edge separation begins, as indicated by the rather sudden decrease in pressure coefficient.

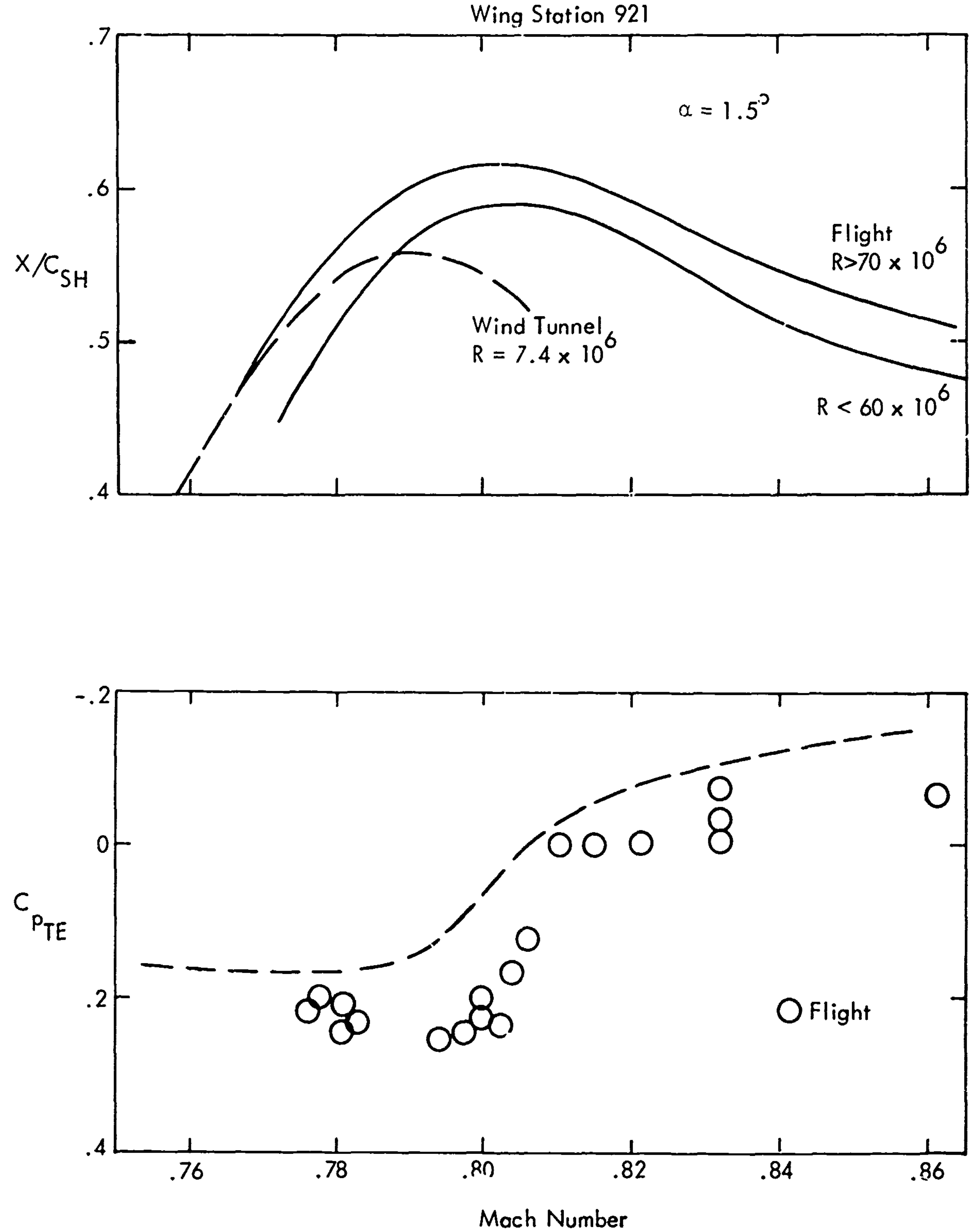

Figure 34. Correlation of Shock Location Change with Trailing-Edge Pressure Recovery

2. IDENTIFICATION OF SHOCK-INDUCED SEPARATION PHENOMENA

Consideration of the measured boundary layer data in conjunction with the pressure distribution and shock location data provides some insight into the reason that no influence of Reynolds number on shock-induced separation is apparent in the data obtained in this investigation. Evidence leading to this insight is reviewed below.

In Reference 1, Pearcey shows quite clearly that scale effects can be anticipated only in those cases where a trailing-edge separation becomes significant downstream of a flow which has reattached behind the terminal shock (or, possibly, does not separate at the shock). Increasing Reynolds number should in all cases tend to suppress this kind of trailing-edge separation, while ample evidence exists to show that increasing Reynolds number has only minor effects on the separation in the immediate vicinity of the shock. Therefore, for any given value of the adverse pressure gradient approaching the trailing edge, it can be anticipated that a Reynolds number can be reached beyond which the trailing-edge separation is suppressed to the point that separation at the shock with no subsequent reattachment will become the dominant factor leading to flow breakdown.

Figures 35 and 36 show the variation with Mach number of several measured quantities which can provide an indication of flow separation. Trailing-edge pressure coefficients (at the top of each figure) generally reach values of approximately 0.2 for unseparated flows, and progressively decrease as trailing-edge separation becomes more severe. Of course, skin friction values must go to zero at the separation point. The flow direction angle measured by the directional Preston tubes is also indicative of approaching separation on a swept wing, and a 180° change in flow direction provides one definition of the separation point in a three-dimensional flow.

The flow direction angle at 75% chord for wing station 592 (Figure 35) indicates small outflow angles in the boundary layer at low Mach numbers and angles of attack. A rather abrupt increase in outflow angle occurs when the Mach number is increased beyond a threshold value which decreases as the angle of attack is increased. The nearly vertical rise in outflow angle must be interpreted as a local separation. The skin friction coefficient at the highest measured flow angles are very small (0.0004 to 0.0006) and also indicate imminent separation. These indications of separated flow at 75% chord precede by substantial margins any significant deterioration in trailing-edge pressure recovery. It appears quite conclusive, therefore, that the final flow breakdown occurs as a result of separation at the shock rather than trailing-edge separation. The data indicate that this condition exists at all Reynolds numbers within the range covered by the flight tests reported here.

The data in Figure 36 for wing station 921 show similar trends in indicated separation, although the difference in the Mach number for separation at 75% chord and at the trailing edge appears to decrease as the angle of attack is increased. This could result either from a more rapid rearward spread of the shock-induced separation or from a more significant development of trailing-edge separation. Unfortunately, the data available are insufficient to determine which of these effects is more likely.

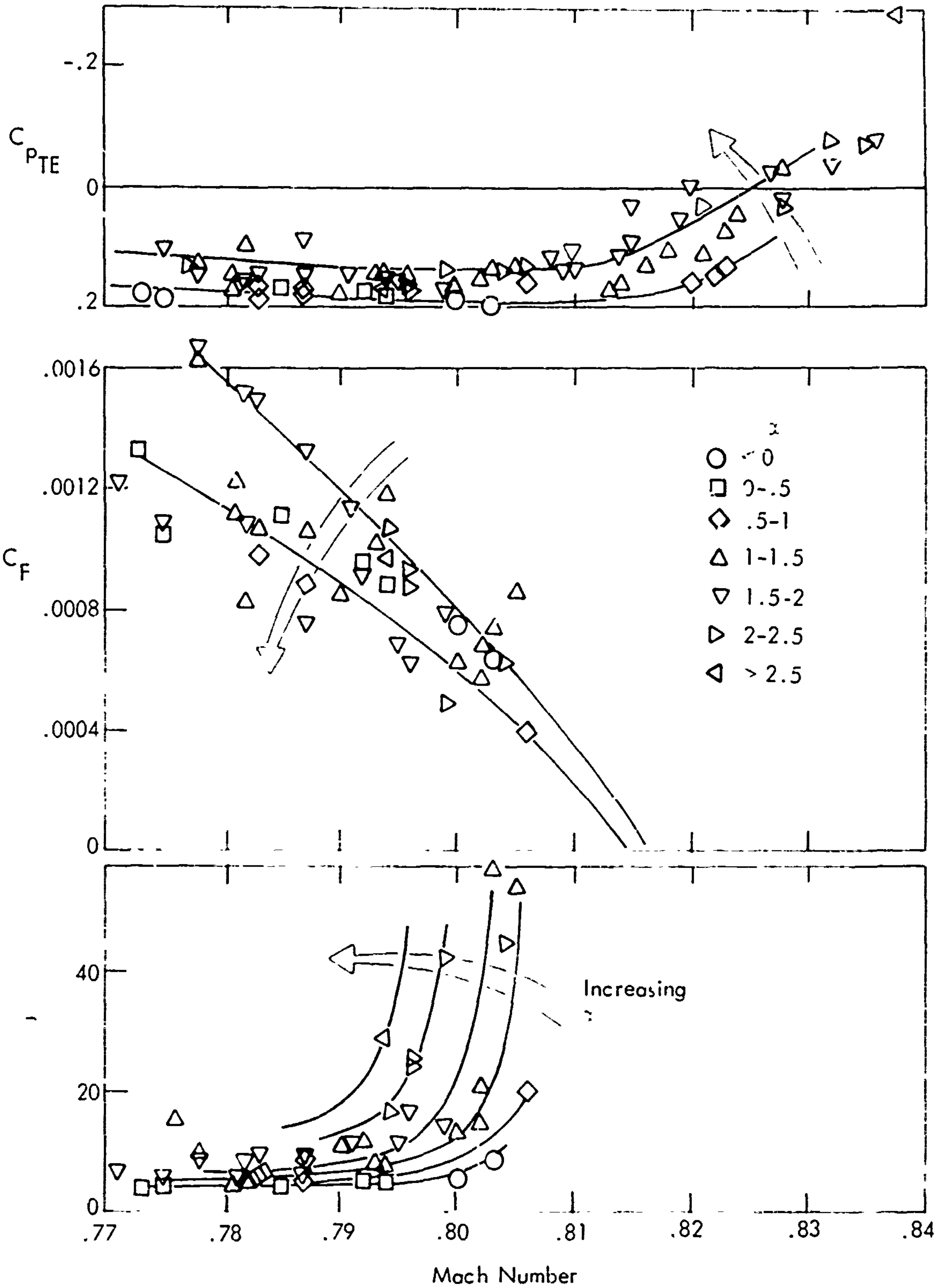

Figure 35. Correlation of Trailing-Edge Pressure Recovery, Skin Friction Coefficient, and Surface Flow Angle at 75% Chord. Wing Station 592.

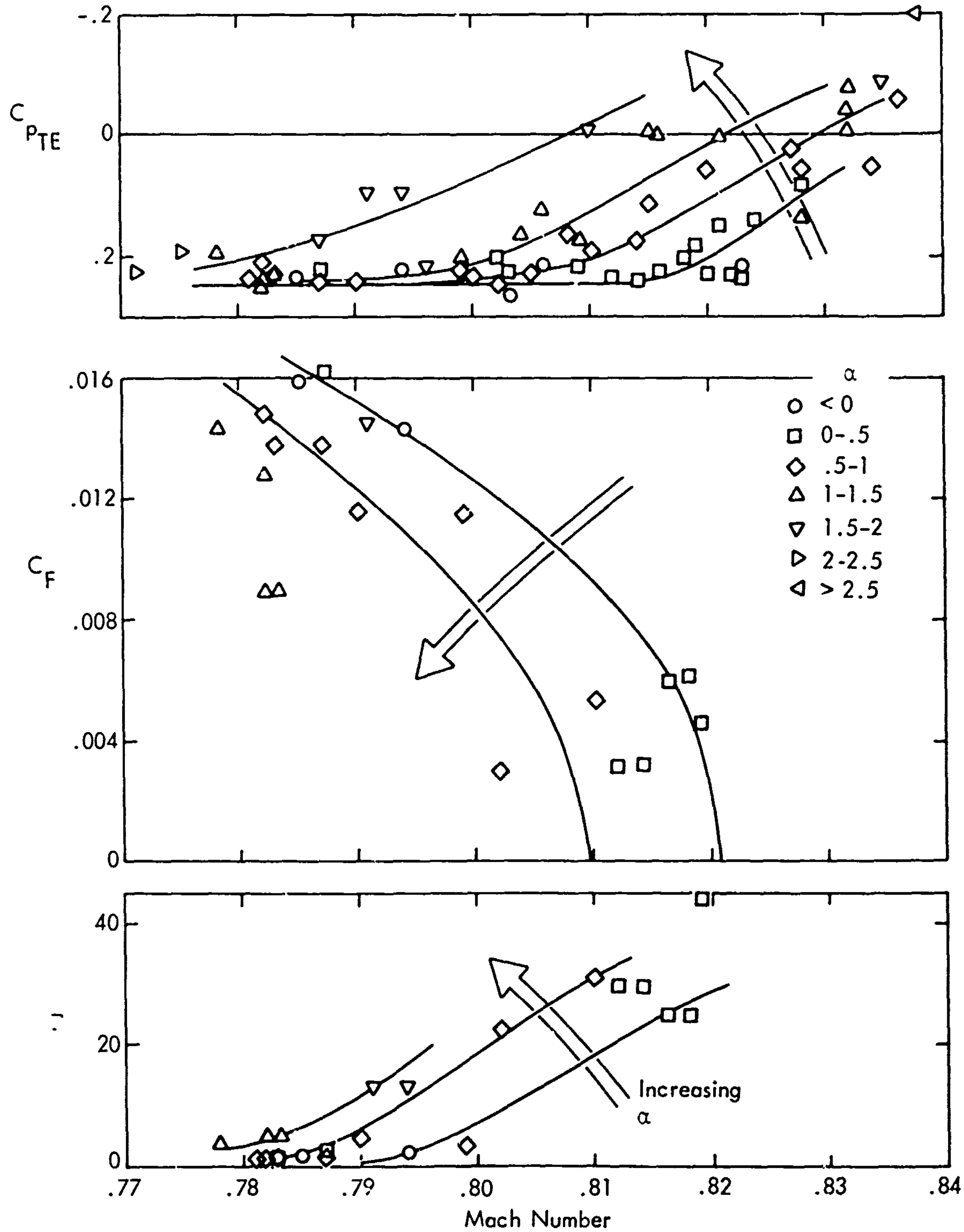

Figure 36. Correlation of Trailing-Edge Pressure Recovery, Skin Friction Coefficient, and Surface Flow Angle at 75% Chord. Wing Station 921

The facts outlined above establish quite clearly that the flow conditions existing on the wing of the C-5A in the range of Reynolds number covered by these flight tests correspond to those classified as Model B by Pearcey in Reference 1. In these flow situations it can be expected that details of flow reattachment behind the shock-induced separation, and the subsequent tendency for the flow to separate again, would depend heavily on local pressure gradients at and immediately behind the reattachment point, since the boundary layer profiles are "weak" in that region. Therefore, an attempt was made to correlate indicated separations with the parameter $(\theta/\rho_e u_e^2)(dp/dx)$ as suggested by Alber in Reference 7. The range of values of the pressure gradient covered by the data available is too small to enable isolation of the factors leading to separation. It would appear that a study of these effects, preferably in a high Reynolds number wind tunnel in which conditions could be rigidly controlled and pressure gradients varied over wide range, would be very profitable in developing a quantitative understanding of scale-effect trends on transonic wings. Results of such a study could contribute significantly to a capability for predicting the probability of scale effects on any given wing design, and ultimately to the development of methods for extrapolation of scale-effect trends if future high Reynolds number tunnels are built with less than full-scale testing capability.

SECTION VI

CONCLUSIONS

Results of wing pressure distribution and boundary layer testing on a C-5A airplane have been studied to investigate scale effects in transonic flow fields at high Reynolds numbers. This study has led to the following general conclusions:

(1) Within the range of Reynolds number covered by the flight tests, flow breakdown results from separation at the shock with no subsequent reattachment rather than from trailing-edge separation.

(2) Because of the mode of flow breakdown, no scale effect on shock location is apparent in the Reynolds number range from approximately 35 to 90 million.

(3) Flight-measured shock locations are aft of those observed in previous wind tunnel tests at a Reynolds number of 7.4×10^6 by as much as 10 to 12% chord at high subsonic Mach numbers.

(4) Comparisons of the measured boundary layer data with several theoretical predictions disclosed no unusual characteristics at these high Reynolds numbers.

TABLE I

SUMMARY OF FLIGHT TEST DATA

TEST POINT	MACH	RN	CL	ALT. (1000FT)	ALPHA	(X/C)S	ME	CF	DSTAR	THETA
284 X1 02-17-41	.363	72.6	.596	2.6						
W.S. 592 FWD					.00	.000	.474	.003063	.343	.246
AFT							.422	.001567	.699	.534
921 FWD					.00	.000	.478	.003390	.246	.176
AFT							.419	.002184	.802	.535
284 X1 02-17-52	.362	72.4	.613	2.6						
W.S. 592 FWD					.00	.000	.476	.003129	.352	.254
AFT							.422	.001616	.716	.551
921 FWD					.00	.000	.475	.003403	.247	.176
AFT							.422	.002248	.805	.541
284 X2 02-26-[illegible]	.399	80.0	.481	2.5						
W.S. 592 FWD					.00	.000	.515	.003026	.319	.227
AFT							.463	.001567	.645	.488
921 FWD					.00	.000	.513	.003227	.226	.160
AFT							.464	.002113	.755	.513
284 X2 02-26-49	.398	79.9	.513	2.5						
W.S. 592 FWD					.00	.000	.516	.002997	.332	.237
AFT							.462	.001558	.651	.492
921 FWD					.00	.000	.517	.003272	.232	.165
AFT							.459	.002140	.745	.505
285 9A1 06-14-40	.796	72.4	.512	24.3						
W.S. 592 FWD					2.30	.649	1.377	.002671	.279	.197
AFT							.913	.000936	1.184	.933
921 FWD					1.90	.625	1.342	.003023	.231	.154

TEST POINT	MACH	RN	CL	ALT. (1000FT)	ALPHA	(X/C)S	ME	CF	DSTAR	THETA
285 9A2 06-19-10	.796	75.4	.508	2[illegible].4						
W.S. 592 FWD					2.40	.630	1.390	.002905	.302	.203
AFT							.914	.000871	1.148	.904
921 FWD					1.80	.600	1.357	.003341	.211	.147
285 9A2 06-19-06	.794	74.5	.519	23.6						
W.S. 592 FWD					3.00	.627	1.397	.002940	.272	.192
AFT							.927	.000968	1.167	.917
921 FWD					1.30	.586	1.367	.003353	.222	.147
285 9A3 06-26-11	.814	77.3	.431	23.2						
W.S. 592 FWD					1.70	.676	1.368	.002874	.260	.182
921 FWD					.55	.655	1.311	.002982	.213	.146
285 9A4 06-32-06	.828	80.9	.425	22.6						
W.S. 592 FWD					2.20	.626	1.404	.003242	.246	.172
AFT							.956	.000379	.247	.594
921 FWD					1.05	.602	1.376	.003581	.197	.137
285 9A5 06-38-38	.834	81.2	.393	22.6						
W.S. 592 FWD					1.70	.651	1.396	.002865	.251	.174
921 FWD					.50	.627	1.336	.002996	.207	.142

TEST POINT	MACH	RN	CL	ALT. (1000FT)	ALPHA	(X/C)S	ME	CF	DSTAR	THETA
285 9A6 06-45-01	.823	78.9	.403	23.0						
W.S. 592 FWD					1.50	.676	1.338	.002924	.256	.179
921 FWD					.50	.652	1.345	.003481	.147	.137
290 7B1A 11-13-20	.782	70.7	.455	24.4						
W.S. 592 FWD					1.50	.600	1.269	.003582	.276	.201
AFT							.899	.001075	.825	.639
921 FWD					1.20	.559	1.319	.003096	.202	.142
AFT							.900	.001246	.973	.548
290 7B1A 11-13-31	.781	70.7	.440	24.3						
W.S. 592 FWD					1.35	.592	1.203	.003124	.279	.200
AFT							.903	.001221	.804	.620
921 FWD					.85	.545	1.266	.003596	.215	.145
AFT							.899	.001353	.955	.547
290 7B1B 11-14-29	.790	73.1	.435	23.7						
W.S. 592 FWD					1.25	.634	1.215	.002587	.297	.215
AFT							.906	.000948	.887	.696
921 FWD					.80	.559	1.270	.003272	.218	.153
AFT							.898	.001230	1.161	.611
290 7B1B 11-14-40	.782	72.3	.434	23.7						
W.S. 592 FWD					1.60	.575	1.215	.002890	.289	.210
AFT							.905	.001081	.828	.641
921 FWD					.85	.524	1.268	.003348	.224	.150
AFT							.898	.001412	.970	.544

TEST POINT	MACH	RN	CL	ALT. (1000FT)	ALPHA	(X/C)S	ME	CF	DSTAR	THETA
290 782D 11-17-39	.783	70.1	.403	24.6						
W.S. 592 FWD					.80	.574	1.189	.003009	.276	.197
AFT							.910	.000975	.807	.620
921 FWD					.35	.523	1.222	.003283	.232	.157
AFT							.905	.001642	1.018	.594
290 782D 11-17-50	.787	71.0	.413	24.4						
W.S. 592 FWD					.90	.579	1.198	.002852	.284	.201
AFT							.913	.000983	.855	.667
921 FWD					.30	.529	1.254	.003204	.223	.156
AFT							.903	.001501	1.053	.580
290 782C 11-19-27	.787	70.3	.398	24.7						
W.S. 592 FWD					1.00	.617	1.203	.003233	.264	.188
AFT							.907	.001064	.785	.600
921 FWD					.70	.568	1.274	.003944	.193	.136
AFT							.908	.001286	.979	.560
290 782C 11-19-16	.783	69.5	.404	24.8						
W.S. 592 FWD					1.00	.598	1.205	.002926	.269	.194
AFT							.909	.001058	.779	.597
921 FWD					.80	.547	1.273	.004017	.205	.139
AFT							.905	.001389	.946	.545
290 782B 11-34-30	.797	72.6	.520	24.2						
W.S. 592 FWD					2.30	.631	1.420	.003198	.297	.200
921 FWD					1.35	.604	1.389	.003715	.223	.148

TEST POINT	MACH	RN	CL	ALT. (100OFT)	ALPHA	(X/C)S	ME	CF	DSTAR	THETA
290 782A 11-35-56	.799	77.7	.479	22.4						
W.S. 592 FWD					1.85	.654	1.391	.003428	.260	.185
AFT							.901	.000893	.978	.797
921 FWD					.80	.625	1.381	.003893	.196	.138
AFT							.902	.001129	1.062	.583
290 782D 11-40-17	.802	74.9	.455	23.5						
W.S. 592 FWD					1.55	.649	1.338	.002997	.277	.197
921 FWD					.75	.608	1.297	.003191	.216	.150
AFT							.901	.000271	1.899	.765
290 782C 11-43-43	.810	75.6	.448	23.5						
W.S. 592 FWD					1.60	.677	1.368	.003192	.263	.186
921 FWD					.80	.562	1.331	.003455	.210	.146
AFT							.916	.000749	1.612	.712
290 782E 11-47-01	.816	76.6	.403	23.4						
W.S. 592 FWD					1.20	.683	1.321	.003082	.260	.183
921 FWD					.25	.658	1.304	.003483	.205	.142
AFT							.911	.000727	1.764	.685
290 782E 11-46-50	.818	76.2	.401	23.6						
W.S. 592 FWD					1.30	.681	1.355	.003206	.259	.182
921 FWD					.50	.656	1.296	.003363	.205	.142
AFT							.933	.000538	1.923	.695

TEST POINT	MACH	RN	CL	ALT. (1000FT)	ALPHA	(X/C)S	ME	CF	DSTAR	THETA
290 782F 11-49-36	.814	75.7	.402	23.6						
W.S. 592 FWD					1.25	.679	1.327	.003176	.298	.201
921 FWD					.35	.650	1.297	.003464	.207	.144
AFT							.913	.000316	1.965	.708
290 782F 11-49-25	.812	74.5	.407	24.0						
W.S. 592 FWD					1.25	.677	1.327	.003141	.293	.191
921 FWD					.45	.647	1.290	.003281	.209	.144
AFT							.914	.000253	1.971	.709
290 782G 11-51-53	.794	70.2	.328	25.0						
W.S. 592 FWD					.30	.638	1.198	.003227	.264	.190
AFT							.916	.000878	.752	.565
921 FWD					-.25	.573	1.199	.003426	.201	.139
AFT							.918	.001429	1.050	.590
290 782H 11-54-06	.792	69.0	.341	25.3						
W.S. 592 FWD					.40	.599	1.201	.003325	.267	.193
AFT							.917	.000954	.764	.578
921 FWD					-.10	.554	1.195	.003353	.207	.145
AFT							.914	.001624	1.039	.588
290 782H 11-54-18	.785	67.8	.361	25.6						
W.S. 592 FWD					.30	.575	1.189	.003391	.269	.195
AFT							.916	.001106	.752	.568
921 FWD					.05	.526	1.184	.003337	.210	.147

TEST POINT	MACH	RN	CL	ALT. (1000FT)	ALPHA	(X/C)S	ME	CF	DSTAR	THETA
290 5A1 10-22-58	.553	49.3	.627	24.8						
W.S. 592 FWD					.00	.000	.758	.003390	.353	.254
AFT							.654	.001397	.780	.616
921 FWD					.00	.000	.755	.003502	.260	.184
290 5A2 10-28-20	.573	49.3	.600	25.8						
W.S. 592 FWD					.00	.000	.789	.003415	.355	.255
AFT							.678	.001263	.798	.632
921 FWD					.00	.000	.789	.003536	.257	.183
290 5B1 10-33-20	.611	54.0	.521	24.9						
W.S. 592 FWD					.00	.000	.833	.003339	.319	.226
AFT							.719	.001271	.725	.556
921 FWD					.00	.000	.838	.003516	.232	.163
290 5B2 10-39-03	.531	53.3	.531	24.8						
W.S. 592 FWD					.00	.000	.821	.003382	.328	.232
AFT							.704	.001160	.745	.575
921 FWD					.00	.000	.816	.003543	.232	.163
290 5C1 10-44-25	.654	57.6	.455	25.1						
W.S. 592 FWD					.00	.000	.899	.003421	.317	.226
AFT							.766	.001350	.696	.528
921 FWD					.00	.000	.900	.003620	.215	.150

TEST POINT	MACH	RN	CL	ALT. (1000FT)	ALPHA	(X/C)S	ME	CF	DSTAR	THETA
290 5C2 10-48-53	.650	58.3	.462	24.7						
W.S. 592 FWD					.00	.000	.893	.003352	.314	.223
AFT							.767	.001257	.719	.552
921 FWD					.00	.000	.888	.003432	.218	.152
290 5D1 10-53-24	.695	61.7	.403	24.8						
W.S. 592 FWD					.00	.000	.958	.003419	.366	.277
AFT							.815	.001414	.730	.561
921 FWD					.00	.000	.956	.003519	.212	.146
290 5D2 10-57-23	.696	63.0	.388	24.4						
W.S. 592 FWD					.00	.000	.965	.003344	.316	.226
AFT							.820	.001385	.738	.572
921 FWD					.00	.000	.960	.003528	.211	.145
290 6A1 11-04-10	.773	68.1	.322	25.0						
AFT							.909	.001329	.716	.542
921 FWD					.00	.497	1.169	.004128	.189	.133
290 6A2 11-09-26	.775	70.2	.294	24.3						
W.S. 592 FWD					.10	.540	1.165	.003525	.249	.177
AFT							.910	.001035	.697	.525
921 FWD					-.35	.496	1.178	.004102	.183	.129

TEST POINT	MACH	RN	CL	ALT. (1000FT)	ALPHA	(X/C)S	ME	CF	DSTAR	THETA
290 681 11-22-28	.800	70.6	.290	25.0						
W.S. 592 FWD					-.10	.623	1.200	.003311	.258	.186
AFT							.919	.000750	.736	.549
921 FWD					-.85	.596	1.202	.003869	.186	.131
290 682 11-27-30	.803	77.3	.263	22.7						
W.S. 592 FWD					-.15	.630	1.196	.003282	.246	.175
AFT							.923	.000631	.707	.535
921 FWD					-1.10	.598	1.201	.003787	.181	.126
310 ONE 08-02-32	.771	80.1	.533	20.5						
W.S. 592 FWD					2.00	.554	1.405	.004509	.261	.183
AFT							.860	.001224	.823	.637
921 FWD					2.00	.521	1.425	.004806	.170	.116
310 TWO 08-06-23	.775	83.5	.452	19.5						
W.S. 592 FWD					2.00	.583	1.243	.003894	.267	.186
AFT							.871	.001086	.792	.608
921 FWD					2.00	.498	1.339	.005462	.165	.112
310 THRE 08-06-34	.787	87.5	.440	18.6						
W.S. 592 FWD					1.60	.618	1.355	.004282	.233	.169
AFT							.866	.000745	.818	.626
921 FWD					1.80	.525	1.385	.004936	.173	.119

TEST POINT	MACH	RN	CL	ALT. (1000FT)	ALPHA	(X/C)S	ME	CF	DSTAR	THETA
310 FOUR 08-09-16	.781	85.5	.406	19.1						
W.S. 592 FWD					1.40	.596	1.217	.003463	.249	.179
AFT							.885	.001114	.754	.571
921 FWD					1.30	.594	1.319	.004747	.170	.115
310 FIVE 08-09-27	.782	86.8	.398	18.7						
W.S. 592 FWD					1.25	.593	1.186	.003436	.267	.185
AFT							.874	.000829	.755	.571
921 FWD					1.20	.594	1.293	.004915	.167	.112
312 9D2B 06-57-10	.815	50.3	.450	33.8						
W.S. 592 FWD					1.75	.675	1.346	.003465	.252	.173
921 FWD					.90	.597	1.344	.003458	.192	.125
312 9D3B 07-04-55	.824	51.6	.404	33.4						
W.S. 592 FWD					1.30	.678	1.365	.003600	.287	.185
921 FWD					.30	.629	1.320	.003564	.178	.116
312 DIAL 07-11-50	.778	44.1	.500	35.9						
W.S. 592 FWD					1.80	.557	1.226	.002786	.322	.221
AFT							.918	.001655	.871	.690
921 FWD					1.35	.487	1.322	.003498	.223	.146

TEST POINT	MACH	RN	CL	ALT. (1000FT)	ALPHA	(X/C)S	ME	CF	DSTAR	THETA
312 D2CL 07-16-35	.809	46.5	.458	35.4						
W.S. 592 FWD					1.70	.657	1.349	.003545	.24[illegible]	.169
921 FWD					1.10	.601	1.329	.003521	.193	.126
312 D2CR 07-20-50	.802	45.3	.415	35.9						
W.S. 592 FWD					1.40	.629	1.291	.003309	.268	.194
AFT							.918	.000672	.964	.787
921 FWD					.40	.573	1.275	.003300	.196	.129
312 9D3A 06-49-50	.832	53.5	.473	32.9						
W.S. 592 FWD					3.10	.629	1.452	.003364	.216	.148
921 FWD					1.40	.517	1.388	.003425	.184	.117
312 9D2B 06-57-10	.815	50.3	.450	33.8						
312 9D2A 06-37-10	.799	48.5	.518	34.3						
W.S. 592 FWD					2.40	.632	1.379	.003427	.255	.175
AFT							.913	.000488	1.356	1.086
921 FWD					1.50	.573	1.353	.003596	.217	.141

TEST POINT	MACH	RN	CL	ALT. (1000FT)	ALPHA	(X/C)S	ME	CF	DSTAR	THETA
312 D2A1 06-43-20	.810	48.7	.528	34.4						
W.S. 592 FWD					1.80	.650	1.425	.003572	.235	.159
921 FWD					1.50	.530	1.401	.003728	.201	.129
312 9C2A 06-07-14	.816	59.6	.485	29.7						
W.S. 592 FWD					2.20	.653	1.410	.003307	.235	.159
921 FWD					1.40	.546	1.416	.003707	.185	.119
312 C2B1 06-16-21	.832	62.4	.415	29.0						
W.S. 592 FWD					1.70	.658	1.384	.003268	.236	.161
921 FWD					1.50	.559	1.369	.003458	.168	.108
312 C2B1 06-16-32	.828	63.3	.416	28.6						
W.S. 592 FWD					1.70	.652	1.384	.003454	.235	.160
921 FWD					.80	.588	1.354	.003584	.173	.111
312 9C1B 06-03-35	.802	55.4	.413	31.1						
W.S. 592 FWD					1.20	.650	1.265	.003238	.271	.195
AFT							.900	.000570	.956	.780
921 FWD					.70	.588	1.316	.003703	.182	.120

TEST POINT	MACH	RN	CL	ALT. (1000FT)	ALPHA	(X/C)S	ME	CF	DSTAR	THETA
312 9C2A 06-07-03	.821	59.0	.465	30.1						
W.S. 592 FWD					2.40	.653	1.387	.003326	.237	.160
921 FWD					1.40	.557	1.385	.00[illegible]77	.185	.119
312 C1A1 06-00-50	.796	55.6	.467	30.8						
W.S. 592 FWD					1.50	.632	1.279	.002993	.274	.193
AFT							.901	.000631	1.004	.831
921 FWD					1.20	.566	1.332	.003447	.205	.134
312 C1A1 06-01-01	.795	55.7	.473	30.8						
W.S. 592 FWD					1.60	.630	1.289	.003204	.272	.192
AFT							.896	.000691	1.151	.903
921 FWD					1.20	.568	1.338	.003546	.201	.132
312 9C1B 06-03-24	.800	54.9	.427	31.2						
W.S. 592 FWD					1.30	.643	1.280	.003040	.266	.191
AFT							.903	.000621	.978	.798
921 FWD					.90	.580	1.310	.003552	.181	.118
312 9C1B 06-03-35	.802	55.4	.413	31.1						

TEST POINT	MACH	RN	CL	ALT. (1000FT)	ALPHA	(X/C)S	ME	CF	DSTAR	THETA
313 B2A1 01-26-05	.806	73.9	.514	23.9						
W.S. 592 FWD					2.10	.657	1.415	.003485	.236	.161
921 FWD					1.20	.593	1.375	.003841	.200	.131
313 B2A1 01-26-16	.804	75.1	.512	23.4						
W.S. 592 FWD					2.15	.657	1.385	.003472	.241	.165
AFT							.914	.000615	1.296	1.042
921 FWD					1.30	.598	1.379	.003884	.199	.130
313 984A 01-40-29	.858	81.3	.326	23.0						
W.S. 592 FWD					1.20	.655	1.369	.003018	.237	.163
921 FWD					.40	.605	1.340	.003109	.200	.130
313 984B 01-53-19	.862	85.6	.298	21.8						
W.S. 592 FWD					1.20	.655	1.360	.003057	.233	.159
921 FWD					.30	.599	1.365	.003612	.189	.124
313 984C 02-04-39	.857	82.3	.248	22.6						
W.S. 592 FWD					.45	.674	1.340	.003235	.233	.161
921 FWD					.20	.655	1.326	.003728	.189	.124

TEST POINT	MACH	RN	CL	ALT. (1000FT)	ALPHA	(X/C)S	ME	CF	DSTAR	THETA
313 9C3A 02-23-39	.861	68.9	.327	27.6						
W.S. 592 FWD					1.50	.632	1.396	.002901	.229	.155
921 FWD					1.70	.555	1.395	.003699	.188	.121
315 9D3A 09-06-45	.823	50.2	.358	33.7						
W.S. 592 FWD					1.00	.689	1.303	.003399	.262	.187
921 FWD					.00	.638	1.314	.003913	.198	.131
315 9D3A 09-06-55	.822	50.3	.362	33.6						
W.S. 592 FWD					1.00	.684	1.307	.003400	.258	.182
921 FWD					.15	.630	1.325	.003996	.200	.131
315 9D3A 09-07-06	.820	50.5	.355	33.5						
W.S. 592 FWD					1.00	.682	1.281	.003209	.257	.180
921 FWD					.15	.630	1.314	.003992	.198	.129
315 9D1A 09-12-35	.794	45.8	.412	35.0						
W.S. 592 FWD					1.10	.604	1.232	.003291	.277	.202
AFT							.926	.001176	.895	.707
921 FWD					.50	.530	1.294	.004170	.210	.139

TEST POINT	MACH	RN	CL	ALT. (1000FT)	ALPHA	(X/C)S	ME	CF	DSTAR	THETA
315 9D1A ,9-12-46	.793	45.7	.415	35.1						
W.S. 592 FWD					1.10	.599	1.236	.003289	.281	.205
AFT							.914	.001010	.870	.685
921 FWD					.60	.523	1.296	.003983	.212	.141
315 9E2A 10-46-09	.815	41.6	.486	37.8						
W.S. 592 FWD					1.75	.652	1.383	.003339	.259	.181
320 6A 05-31-04	.803	92.7	.464	17.5						
W.S. 592 FWD					1.30	.678	1.307	.003208	.242	.167
AFT							.898	.000743	1.110	.877
921 FWD					.30	.630	1.291	.003578	.196	.132
320 6B 05-44-15	.819	87.3	.439	19.5						
W.S. 592 FWD					1.50	.680	1.347	.003320	.247	.171
921 FWD					.30	.651	1.328	.003781	.197	.133
AFT							.927	.000376	1.873	.757
320 6B 05-44-27	.805	86.5	.460	19.3						
W.S. 592 FWD					1.40	.678	1.344	.003285	.243	.168
AFT							.918	.000848	1.091	.857
921 FWD					.60	.630	1.317	.003757	.193	.129

TEST POINT	MACH	RN	CL	ALT. (1000FT)	ALPHA	(X/C)S	ME	CF	DSTAR	THETA
320 6C2 09-15-05	.808	67.3	.496	25.9						
W.S. 592 FWD					1.90	.680	1.369	.003106	.245	.167
921 FWD					.90	.630	1.357	.003749	.200	.133
320 6D 09-22-48	.827	69.2	.448	25.8						
W.S. 592 FWD					1.80	.655	1.386	.003070	.228	.154
921 FWD					.60	.580	1.391	.003854	.192	.127
320 6D 09-22-59	.820	69.8	.461	25.4						
W.S. 592 FWD					1.70	.651	1.367	.003229	.232	.157
921 FWD					.80	.583	1.377	.004053	.189	.126
320 6E 09-36-10	.828	67.5	.405	26.5						
W.S. 592 FWD					1.45	.658	1.369	.003216	.240	.165
921 FWD					.40	.629	1.360	.003939	.192	.128
320 6E 09-36-21	.809	65.8	.432	26.5						
W.S. 592 FWD					1.10	.681	1.316	.003467	.254	.174
921 FWD					.30	.636	1.332	.004096	.195	.130

TEST POINT	MACH	RN	CL	ALT. (1000FT)	ALPHA	(X/C)S	ME	CF	DSTAR	THETA
321 6F 03-18-56	.836	61.0	.416	29.3						
W.S. 592 FWD					1.90	.630	1.362	.002954	.237	.160
921 FWD					.90	.550	1.382	.003573	.196	.130
321 6G 03-25-17	.791	53.4	.504	31.2						
W.S. 592 FWD					1.80	.625	1.381	.003658	.237	.163
AFT							.897	.001138	1.223	.960
921 FWD					1.50	.570	1.479	.005009	.179	.116
AFT							.898	.001491	1.500	.748
321 6G 03-25-28	.794	54.3	.494	30.9						
W.S. 592 FWD					2.00	.640	1.380	.003683	.252	.179
AFT							.899	.001055	1.131	.877
921 FWD					1.50	.584	1.471	.004871	.185	.124
AFT							.915	.001509	1.618	.768
321 6H 03-27-22	.782	52.4	.444	31.4						
W.S. 592 FWD					1.60	.593	1.227	.003433	.255	.182
AFT							.904	.001509	.862	.680
921 FWD					1.30	.522	1.309	.004277	.192	.131
AFT							.879	.000852	.928	.532
321 6H 03-27-33	.783	52.6	.466	31.3						
W.S. 592 FWD					1.60	.598	1.216	.003289	.280	.201
AFT							.904	.001493	.873	.682
921 FWD					1.30	.527	1.350	.004370	.205	.138
AFT							.882	.001031	1.031	.579

TEST POINT	MACH	RN	CL	ALT. (1000FT)	ALPHA	(X/C)S	ME	CF	DSTAR	THETA
321 13A 03-43-57	.832	49.8	.430	34.2						
W.S. 592 FWD					2.00	.628	1.422	.003429	.225	.154
AFT							.877	.000422	1.127	.940
921 FWD					1.50	.537	1.431	.004099	.197	.130
321 13A 03-44-09	.821	49.6	.406	34.0						
W.S. 592 FWD					1.40	.600	1.389	.003645	.244	.170
921 FWD					.70	.620	1.374	.004007	.198	.134
321 13D 03-48-43	.821	49.6	.406	34.0						
W.S. 592 FWD					1.30	.578	1.141	.002601	.283	.202
921 FWD					.50	.493	1.222	.003685	.247	.184
AFT							.881	.000675	1.021	.535
321 13D 03-48-54	.778	43.2	.442	36.0						
W.S. 592 FWD					1.30	.555	1.198	.003201	.278	.201
AFT							.917	.001632	.823	.643
921 FWD					1.20	.459	1.291	.004060	.230	.153
AFT							.883	.001384	.978	.550
321 13F 05-06-20	.779	35.2	.497	40.9						
W.S. 592 FWD					1.80	.578	1.168	.001318	.338	.241
921 FWD					1.60	.511	1.297	.002530	.244	.164

TEST POINT			MACH	RN	CL	ALT. (1000FT)	ALPHA	(X/C)S	ME	CF	DSTAR	THETA
321	[illegible]	05-06-32	[illegible]	35.3	.478	40.9						
	W.S.	592 FWD					1.50	.577	1.191	.001644	.330	.241
		921 FWD					1.40	.520	1.286	.002875	.248	.164
321	13C	05-10-19	.835	40.5	.498	39.2						
	W.S.	59. FWD					2.20	.612	1.396	.003593	.231	.154
		921 FWD					1.70	.452	1.345	.003490	.206	.136
321	13E	05-10-29	.838	41.9	.510	38.5						
	W.S.	592 FWD					3.20	.542	1.481	.003147	.194	.147
		921 FWD					2.80	.410	1.132	.001116	.272	.173
321	13B	05-15-59	.869	51.0	.367	34.7						
	W.S.	592 FWD					2.10	.600	1.463	.003087	.193	.150
		921 FWD					1.90	.490	1.465	.003816	.190	.127
321	13B	05-16-11	.866	53.7	.383	33.4						
	W.S.	592 FWD					2.40	.602	1.443	.003132	.179	.133
		921 FWD					1.80	.492	1.459	.003825	.175	.113

TEST POINT	MACH	RN	CL	ALT. (1000FT)	ALPHA	(X/C)S	ME	CF	DSTAR	THETA
321 13FR 05-27-46	.776	36.5	.461	39.9						
W.S. 592 FWD					1.20	.552	1.331	.004889	.271	.189
AFT							1.007	.003068	.747	.584
921 FWD					1.30	.456	1.228	.002556	.258	.172
321 13C 05-29-31	.878	50.3	.340	35.3						
W.S. 592 FWD					1.90	.607	1.453	.002978	.221	.155
921 FWD					1.70	.530	1.450	.002681	.191	.127
321 14 05-39-56	.887	68.8	.201	27.7						
W.S. 592 FWD					1.20	.683	1.377	.002975	.211	.146
921 FWD					.30	.311	1.381	.003624	.184	.122
312 D1AR 07-26-50	.792	44.6	.472	35.9						
W.S. 592 FWD					1.50	.602	1.250	.002810	.286	.201
AFT							.900	.000917	1.123	.878
921 FWD					1.20	.553	1.336	.003783	.213	.142
312 9B1A 07-59-20	.748	57.4	.489	28.4						
W.S. 592 FWD					.50	.500	1.090	.002924	.331	.234
AFT							.888	.001567	.819	.641
921 FWD					.70	.400	1.038	.003175	.217	.149

TEST POINT	MACH	RN	CL	ALT. (1000FT)	ALPHA	(X/C)S	ME	CF	DSTAR	THETA
312 9818 08-02-50	.787	62.6	.472	27.6						
W.S. 592 FWD					1.60	.602	1.213	.002453	.300	.216
AFT							.906	.001318	.912	.726
921 FWD					1.00	.543	1.288	.003197	.209	.138
312 982A 07-55-50	.806	65.5	.367	27.0						
W.S. 592 FWD					.90	.659	1.231	.003068	.267	.189
AFT							.911	.000[illegible]93	.907	.728
921 FWD					.00	.602	1.246	.003[illegible]65	.179	.116
312 983A 07-41-05	.817	69.2	.399	26.0						
W.S. 592 FWD					1.20	.683	1.297	.003380	.307	.165
921 FWD					.30	.634	1.285	.003468	.193	.100
312 983B 07-46-50	.829	73.6	.325	24.8						
W.S. 592 FWD					.80	.702	1.263	.003129	.313	.167
921 FWD					-.35	.653	1.253	.003458	.174	.097
- -	.000	.0	.000	.0						

TABLE II
TYPICAL SKIN FRICTION CALCULATIONS
USING THE VAN DRIEST II AND SPALDING-CHI THEORIES

FLIGHT	RUN	TIME	CF(EXP)	CF(X)	CF(THETA)	CF(VAN DRIEST)	M-INF	RN	CL
284	X1	02 17 41	.0019092	.0021000	.0019772	.0018413	.363	72.623	.596
284	X1	02 17 41	.0020821	.0021673	.0020894	.0018856	.363	72.623	.596
284	X1	02 17 41	.0011931	.0019626	.0017607	.0016197	.363	72.623	.596
284	X1	02 17 41	.0016884	.0020188	.0017581	.0017557	.363	72.623	.596
284	X1	02 17 52	.0019290	.0020979	.0019639	.0018879	.362	72.383	.613
284	X1	02 17 52	[illegible]1066	.0021670	.0020890	.0019772	.362	72.383	.613
234	X1	02 17 52	[illegible]261	.0019611	.0017495	.0016900	.362	72.383	.613
284	X1	02 17 52	.0017[illegible]93	.0020164	.0017522	.0018470	.362	72.383	.613
284	X2	02 26 35	.0019511	.0020785	.0019784	.0018962	.399	80.034	.481
234	X2	02 26 35	.0020936	.0021476	.0020993	.0019546	.399	80.034	.481
284	X2	02 26 35	.0012087	.0019367	.0017594	.0017501	.399	80.034	.481
234	X2	02 26 35	.0016255	.0019931	.0017417	.0018445	.399	80.034	.481
284	X2	02 26 49	.0019166	.0020785	.0019638	.0018806	.398	79.889	.513
284	X2	02 26 49	.0020850	.0021463	.0020870	.0019318	.398	79.889	.513
234	X2	02 26 49	.0012000	.0019398	.0017583	.0017237	.398	79.889	.513
284	X2	02 26 49	.0016696	.0019965	.0017501	.0018464	.398	79.889	.513
285	9A1	06 14 40	.0018754	.0021075	.0020593	.0019493	.796	72.397	.512
285	9A1	06 14 40	.0021161	.0021851	.0021555	.0020011	.796	72.397	.512
285	9A1	06 14 40	.0008300	.0019611	.0016272	.0020207	.796	72.397	.512
285	9A2	06 19 10	.0020383	.0020924	.0020308	.0019288	.796	75.351	.508
285	9A2	06 19 10	.0023443	.0021630	.0021483	.0020017	.796	75.351	.508
285	9A2	06 19 10	.0007718	.0019673	.0016224	.0020099	.796	75.351	.508
285	9A2	06 19 06	.0020521	.0020967	.0020551	.0019184	.794	74.539	.519
285	9A2	06 19 06	.0023402	.0021699	.0021541	.0019921	.794	74.539	.519
285	9A2	06 19 06	.0008416	.0019703	.0016219	.0019805	.794	74.539	.519

FLIGHT	RUN	TIME	CF(EXP)	CF(X)	CF(THETA)	CF(VAN DRIEST)	M-INF	RN	CL
230	5C2	10 48 53	.0023167	.0021491	.0020673	.0023017	.650	58.261	.462
230	5C2	10 48 53	.0023664	.0022319	.0022158	.0022774	.650	58.261	.462
230	5C2	10 48 53	.0010282	.0020102	.0018041	.0021329	.650	58.261	.462
230	5D1	10 53 24	.0023686	.0021767	.0020242	.0019609	.695	61.750	.403
230	5D1	10 53 24	.0024837	.0022250	.0022219	.0022181	.695	61.750	.403
230	5D1	10 53 24	.0011849	.0020030	.0017901	.0021144	.695	61.750	.403
230	5D2	10 57 23	.0023425	.0021504	.0020639	.0021231	.696	63.040	.388
230	5D2	10 57 23	.0024829	.0022209	.0022198	.0021980	.696	63.040	.388
230	5D2	10 57 23	.0011547	.0019968	.0017769	.0021056	.696	63.040	.388
230	6A1	11 04 10	.0029146	.0022355	.0022326	.0021014	.773	68.148	.322
230	6A1	11 04 10	.0011415	.0019891	.0017831	.0020437	.773	68.148	.322
230	6A2	11 09 26	.0025241	.0021172	.0021084	.0020922	.775	70.197	.294
230	6A2	11 09 26	.0028871	.0021994	.0022363	.0020673	.775	70.197	.294
230	6A2	11 09 26	.0009908	.0019825	.0017853	.0020330	.775	70.197	.294
230	6B1	11 22 28	.0024069	.0021371	.0021147	.0019993	.800	70.601	.290
230	6B1	11 22 28	.0028091	.0022059	.0022383	.0020632	.800	70.601	.290
230	6B1	11 22 28	.0006662	.0019672	.0017767	.0020480	.800	70.601	.290
230	6B2	11 27 30	.0024031	.0021141	.0021081	.0019865	.803	77.336	.263
230	6B2	11 27 30	.0027605	.0021846	.0022265	.0020332	.803	77.336	.263
230	6B2	11 27 30	.0005602	.0019679	.0017617	.0020147	.803	77.336	.263

FLIGHT	RUN	TIME	CF(EXP)	CF(X)	CF(THETA)	CF(VAN DRIEST)	M-INF	RN	CL
312	D1AL	07 11 50	.0019798	.0022232	.0021566	.0022563	.778	44.052	.500
312	D1AL	07 11 50	.0024252	.0022975	.0023070	.0022513	.778	44.052	.500
312	D1AL	07 11 50	.0014351	.0020821	.0018159	.0022868	.778	44.052	.500
312	D2CL	07 16 35	.0025764	.0022160	.0022441	.0021582	.809	46.543	.458
312	D2CL	07 16 35	.0025596	.0022928	.0023570	.0022350	.809	46.543	.458
312	D2CR	07 20 50	.0023810	.0022318	.0022128	.0021492	.802	45.290	.415
312	D2CR	07 20 50	.0023956	.0023026	.0023597	.0022769	.802	45.290	.415
312	D2CR	07 20 50	.0006048	.0020808	.0017731	.0022702	.802	45.290	.415
312	9D3A	06 49 50	.0025071	.0022016	.0022754	.0020442	.832	53.473	.473
312	9D3A	06 49 50	.0025475	.0022701	.0023653	.0021401	.832	53.473	.473
312	9D2A	06 37 10	.0024372	.0022070	.0022208	.0021045	.799	48.451	.518
312	9D2A	06 37 10	.0025563	.0022632	.0023032	.0021803	.799	48.451	.519
312	9D2A	06 37 10	.0004377	.0020701	.0016711	.0022055	.799	48.451	.518
312	D2A1	06 43 20	.0025914	.0022055	.0022540	.0021042	.810	48.708	.528
312	D2A1	06 43 20	.0026986	.0022774	.0023297	.0021755	.810	48.708	.528

REFERENCES

1. Pearcey, H. H., Osborne, J., and Haines, A. B., "The Interaction Between Local Effects at the Shock and Rear Separation - A Source of Significant Scale Effects in Wind-Tunnel Tests on Airfoils and Wings," AGARD C.P. No. 35, September 1968.

2. Cahill, J. F., "Simulation of Full-Scale-Flight Aerodynamic Characteristics by Tests in Existing Transonic Wind Tunnels," AGARD C.P. No. 83, April 1971.

3. Rajaratnam, N., and Muralidhar, D., "Yaw Probe Used as Preston Tube," Aeronautical Journal, Vol. 72, Number 696, December 1968.

4. Patel, V. C., "Calibration of the Preston Tube and Limitations on Its Use in Pressure Gradients," Journal of Fluid Mechanics (1965), Vol. 23, Part 1.

5. Bolen, G. C., "Investigation of Static Pressure Distribution at High Mach and Reynolds Numbers of a 0.040 Scale Model in the AEDC 16-foot Transonic Wind Tunnel; High Speed Pressure - Series 2A," Report LG1T6-1-43, Lockheed-Georgia Co., April 1968.

6. Burdges, K. P., "A Synthesis of Transonic, 2-D Airfoil Technology," AIAA Paper No. 73-792, August 1973.

7. Nash, J. F., and Scruggs, R. M., "Three-Dimensional Compressible Boundary-Layer Computations for a Finite Swept Wing," NASA CR-112158.

8 Van Driest, E. R., "Turbulent Boundary Layer in Compressible Fluids," Journal of the Aeronautical Sciences, Vol. 18, No. 3, March 1951.

9. Stevens, W. A., Groadia, S. H., and Braden, J. A., "Mathematical Model for Two-Dimensional Multi-Component Airfoils in Viscous Flow," NASA CR-1843, July 1971.

10. Komar, J. J., "Improved Turbulent Skin-Friction Coefficient Predictions Utilizing the Spalding-Chi Method," Douglas Report DAC-59801, November 1966.

11. Van Driest, E. R., "The Problem of Aerodyn ic Heating," Aeronautical Engineering Review, October 1956.

12. Alber, E. E., Bacon, J. W., Masson, B. S., and Collins, D. J., "An Experimental Investigation of Turbulent Transonic Viscous-Inviscid Interactions," AIAA Paper No. 71-565, June 1971.

U S Government Printing Office 1974 657-015 228